



UNIVERSITY OF LEEDS

This is a repository copy of *Cooling history of Earth's core with high thermal conductivity*.

White Rose Research Online URL for this paper:

<http://eprints.whiterose.ac.uk/85599/>

Version: Accepted Version

---

**Article:**

Davies, CJ (2015) Cooling history of Earth's core with high thermal conductivity. *Physics of the Earth and Planetary Interiors*, 247. 65 - 79. ISSN 0031-9201

<https://doi.org/10.1016/j.pepi.2015.03.007>

---

(c) 2015, Elsevier. Licensed under the Creative Commons Attribution-NonCommercial-NoDerivatives 4.0 International <http://creativecommons.org/licenses/by-nc-nd/4.0/>

**Reuse**

Unless indicated otherwise, fulltext items are protected by copyright with all rights reserved. The copyright exception in section 29 of the Copyright, Designs and Patents Act 1988 allows the making of a single copy solely for the purpose of non-commercial research or private study within the limits of fair dealing. The publisher or other rights-holder may allow further reproduction and re-use of this version - refer to the White Rose Research Online record for this item. Where records identify the publisher as the copyright holder, users can verify any specific terms of use on the publisher's website.

**Takedown**

If you consider content in White Rose Research Online to be in breach of UK law, please notify us by emailing [eprints@whiterose.ac.uk](mailto:eprints@whiterose.ac.uk) including the URL of the record and the reason for the withdrawal request.



[eprints@whiterose.ac.uk](mailto:eprints@whiterose.ac.uk)  
<https://eprints.whiterose.ac.uk/>

# Cooling history of Earth's core with high thermal conductivity

Christopher J. Davies<sup>a,b,\*</sup>

<sup>a</sup>*School of Earth and Environment, University of Leeds, Leeds LS2 9JT, UK*

<sup>b</sup>*Institute of Geophysics and Planetary Physics, Scripps Institution of Oceanography, University of California San Diego, 9500 Gilman Drive, La Jolla, CA 92093-0225*

---

## Abstract

Thermal evolution models of Earth's core constrain the power available to the geodynamo process that generates the geomagnetic field, the evolution of the solid inner core and the thermal history of the overlying mantle. Recent upward revision of the thermal conductivity of liquid iron mixtures by a factor of 2–3 has drastically reduced the estimated power available to generate the present-day geomagnetic field. Moreover, this high conductivity increases the amount of heat that is conducted out of the core down the adiabatic gradient, bringing it into line with the highest estimates of present-day core-mantle boundary heat flow. These issues raise problems with the standard scenario of core cooling in which the core has remained completely well-mixed and relatively cool for the past 3.5 Ga. This paper presents cooling histories for Earth's core spanning the last 3.5 Ga to constrain the thermodynamic conditions corresponding to marginal dynamo evolution, i.e. where the ohmic dissipation remains just positive over time. The radial variation of core properties is represented by polynomials, which gives good agreement with radial profiles derived from seismological and mineralogical data and allows the governing energy and entropy equations to be solved analytically. Time-dependent evolution of liquid and solid light element concentrations, the melting curve and gravitational energy are calculated for an Fe-O-S-Si model of core chemistry. A suite of cooling histories are presented by varying the inner core boundary density jump, thermal conductivity and amount of radiogenic heat production in the core. All models where the core remains superadiabatic predict an inner core age of  $\lesssim 600$  Myr, about two times younger than estimates based on old (lower) thermal conductivity estimates, and core temperatures that exceed present estimates of the lower mantle solidus prior to the last 0.5–1.5 Ga. Allowing the top of the core to become strongly subadiabatic in recent times pushes the onset of inner core nucleation back to  $\sim 1.5$  Gyr, but the ancient core temperature still implies a partially molten mantle prior to  $\sim 2$  Ga. Based on these results, the scenario of a long-lived basal magma ocean and subadiabatic present-day core seems hard to avoid.

*Keywords:* Geodynamo, outer core, thermal history, inner core age

---

\*Corresponding author

*Email address:* c.davies@earth.leeds.ac.uk; tel: +44 (0) 113 3435543 (Christopher J. Davies)

## 1. Introduction

The paleomagnetic observation that the geomagnetic field has persisted for at least the last 3.45 Ga (Biggin et al., 2009; Tarduno et al., 2010) provides remarkable insight into the dynamics and evolution of Earth’s deep interior. The field is generated in Earth’s liquid outer core by a dynamo process in which the kinetic energy of fluid motions is converted into magnetic energy. The power source that keeps the core fluid moving is thought to derive from the slow cooling of the whole planet, and in particular the solid mantle, which sets the amount of heat flowing across the core-mantle boundary (CMB) (e.g. Gubbins et al., 1979). A viable cooling history for the Earth must involve sufficient CMB heat flow to power the geodynamo for the last  $\sim 3.5$  Ga. Moreover, the thermal evolution of the core places important constraints on the growth history of the solid inner core (e.g. Nimmo, 2007) and the evolution of the mantle (e.g. Buffett, 2002).

The standard procedure for calculating core cooling histories assumes that it is possible to average out rapid fluctuations associated with convection and the geodynamo process to leave equations describing the long-term evolution of the core (e.g. Gubbins et al., 1979; Braginsky and Roberts, 1995; Buffett et al., 1996; Labrosse et al., 1997; Gubbins et al., 2003). The outer core fluid, a mixture of iron together with some lighter elements, is supposed to be compositionally uniform and follow an adiabatic temperature profile as would be the case if it were vigorously convecting. The resulting model, which is employed in the present study, relates the CMB heat flow  $Q_{\text{cmb}}$ , to the dissipation resulting from field generation, the Ohmic heating  $E_J$ . The heat sources that make good the imposed CMB heat flow arise from the presence of any radiogenic elements in the core (e.g. Nimmo et al., 2004) and cooling by the mantle. Cooling leads to freezing of the solid inner core from the centre of the Earth outwards, which releases latent heat due to the phase change (Verhoogen, 1961) and leaves the light component of the iron mixture in the liquid phase where it is free to rise and provide a source of compositional buoyancy (Braginsky, 1963). Cooling also causes contraction of the core, but the associated heat sources are much smaller than those arising from inner core growth (Gubbins et al., 2003).

The relationship between  $Q_{\text{cmb}}$  and  $E_J$  depends on properties of the core fluid at the relevant pressure-temperature conditions. Advances in theoretical and experimental mineral physics techniques over the last few years have significantly improved estimates of core properties such as the melting temperature and composition (Alfè et al., 2007; Hirose et al., 2013). One quantity of particular importance is the thermal conductivity,  $k$ . Recent studies have presented the first calculations of  $k$  at core pressures and temperatures for both pure iron (Pozzo et al., 2012) and liquid iron mixtures (de Koker et al., 2012; Pozzo et al., 2013; Gomi et al., 2013). These studies used different techniques and yet all found  $k$  at the CMB in the range 80–110 W m<sup>-1</sup> K<sup>-1</sup>, increasing up to 140–160 W m<sup>-1</sup> K<sup>-1</sup> at the inner core boundary (ICB). These values are 2–3 times higher than those commonly found in the literature, e.g.  $k = 28$  W m<sup>-1</sup> K<sup>-1</sup> (Stacey and Loper, 2007) and  $k = 63$  W m<sup>-1</sup> K<sup>-1</sup> (Stacey and Anderson, 2001).

Nimmo (2007) summarises the results from core cooling models that used the old (low) values of thermal conductivity. The main conclusions are: 1) cooling can provide enough

43 power to keep the core continually well-mixed and sustain the geomagnetic field over the last  
 44 3.5 Ga; 2) the inner core is a relatively young feature of the planet, around 1 billion years  
 45 old; 3) the early core temperature was within the range of estimates for the lower mantle  
 46 solidus. Remarkably, the seemingly innocuous change in  $k$  has raised significant problems  
 47 with this picture.

48 Increasing the thermal conductivity enhances the heat  $Q_k = 4\pi k(r_o)r_o^2 dT_a/dr|_{r=r_o}$  that  
 49 must be conducted across the CMB (radius  $r = r_o$ ) down the adiabatic gradient  $dT_a/dr|_{r=r_o}$ :  
 50 for  $k = 63 \text{ W m}^{-1} \text{ K}^{-1}$   $Q_k \approx 9 \text{ TW}$  while  $k = 100 \text{ W m}^{-1} \text{ K}^{-1}$  gives  $Q_k \approx 15 \text{ TW}$  (Pozzo  
 51 et al., 2012). Here  $r$  is radius and  $T_a$  is the adiabatic temperature, defined below.  $Q_{\text{cmb}}$  is  
 52 rather poorly known, even for the present-day. Using the range  $Q_{\text{cmb}} = 7 - 17 \text{ TW}$  estimated  
 53 by Lay et al. (2009) and Nimmo (2014) implies that the top of the core is either neutrally  
 54 stable ( $Q_{\text{cmb}} = Q_k$ ) or subadiabatic ( $Q_{\text{cmb}} < Q_k$ ). Subadiabatic conditions may give rise  
 55 to stable stratification below the CMB (Labrosse et al., 1997; Lister and Buffett, 1998;  
 56 Pozzo et al., 2012; Nakagawa and Tackley, 2013; Gomi et al., 2013), which has significant  
 57 implications for explaining the geomagnetic secular variation because it precludes radial  
 58 motion at the top of the core (e.g. Gubbins, 2007).

59 Heat conducted down the adiabat is not available to drive core convection and so in-  
 60 creasing  $k$  also decreases the power available to the dynamo. Pozzo et al. (2012) found  
 61 that maintaining the same magnetic field with the higher conductivity would require the  
 62 core to cool roughly twice as rapidly, thus making the inner core a much younger feature  
 63 of the planet, perhaps only 300 Myrs old. A younger inner core means that purely ther-  
 64 mal convection, which is less efficient than chemically-driven convection (Lister and Buffett,  
 65 1995; Gubbins et al., 2004), must drive the geodynamo for longer. These issues have led  
 66 to concerns that cooling at early times may not have been rapid enough to power the core  
 67 dynamo (Buffett, 2012). Indeed, Ziegler and Stegman (2013) suggested that the early geo-  
 68 magnetic field may have been generated in a magma ocean at the base of the mantle. On  
 69 the other hand, Nakagawa and Tackley (2014) found that the mantle cools the core too  
 70 rapidly in some mantle convection models (the present-day inner core radius is smaller than  
 71 the model prediction) and introduced a primordial layer of dense material at the base of the  
 72 mantle in order to match the present-day ICB radius. The extent to which the new con-  
 73 ductivity values modify previous conclusions regarding core thermal evolution is therefore  
 74 rather uncertain at present. Resolving this issue is clearly fundamental to the basic model  
 75 of long-term geodynamo evolution.

76 In this study we seek to constrain viable core thermal histories by searching for the  
 77 conditions that give a marginal dynamo evolution, i.e. models with the minimum  $E_J$  such  
 78 that  $E_J \geq 0$  for all time. The value of  $E_J$  for the geodynamo is probably much greater  
 79 than zero (Roberts et al., 2003), but its value is very poorly known, partly because the  
 80 toroidal component of the field does not emerge from the core and partly because the major  
 81 contributions to  $E_J$  are thought to arise on small lengthscales (Gubbins, 1975). Lower  
 82 values of  $E_J$  result in slower core cooling and so the models here are conservative in this  
 83 sense. Attention is focused on the predicted inner core age, which is estimated to be 1 Gyr  
 84 using old (low) thermal conductivity estimates (Labrosse et al., 2001), and the ancient core  
 85 temperature. Estimates of the lower mantle solidus go from  $3570 \pm 200 \text{ K}$  (Nomura et al.,

2014) to  $\sim 4150 \pm 150$  K (e.g. Fiquet et al., 2010; Andrault et al., 2011). Core temperatures exceeding these values indicate partial melting of the lowermost mantle.

Most of the models in this study are constrained such that the whole core is superadiabatic ( $Q_{\text{cmb}} > Q_{\text{k}}$ ). If  $Q_{\text{cmb}} < Q_{\text{k}}$  a stable layer may develop below the CMB in which the assumptions of an adiabatic temperature profile and well-mixed light element concentration are not strictly valid. Instead, this situation requires the solution of conduction equations in the layer (Labrosse et al., 1997; Lister and Buffett, 1998). On the other hand, the whole core could remain adiabatic and well-mixed when  $Q_{\text{cmb}} < Q_{\text{k}}$  if compositional convection can carry the excess heat downwards (Loper, 1978). Discriminating between the possibilities requires detailed analysis of the buoyancy sources that drive convection (Davies and Gubbins, 2011; Gomi et al., 2013), while the stability of the layer may be influenced by penetration of the underlying convection or double-diffusive instabilities (Manglik et al., 2010). Some models in this study correspond to a dynamo that is always marginal, which can cause the top of the core to become subadiabatic. We do not analyse the static stability of subadiabatic regions in these models and assume any stable regions that may form are thin enough not to influence the calculated entropy, i.e. that the assumptions of adiabaticity and well-mixed concentration continue to hold. Maintaining a given dissipation requires the core to cool faster if a stable region is present, implying younger inner core ages and higher ancient core temperatures than those estimated below.

This paper is organised as follows. In section 2 we outline the model equations and define a new polynomial representation of the radial core structure that is designed to give good agreement with present-day profiles derived from seismological and mineralogical data. We also describe a method to compute the depression of the pure iron melting point due to the presence of multiple light element species. The proposed radial core structure and melting curve are compared to previous studies in section 3. In section 4 we present a selection of core cooling models by varying the most uncertain input parameters: the density jump at the ICB, the thermal conductivity and the amount of radiogenic heating. Discussion and conclusions are presented in section 5. The main result of this work is contained in Figure 7.

## 2. Methods

The governing equations describing global energy and entropy balance have been described in detail elsewhere (Gubbins et al., 2003, 2004; Nimmo, 2014) and only an outline is given here. The equivalence of alternative formulations (e.g. Buffett et al., 1996; Labrosse et al., 1997) to the present model was shown by Lister (2003). Averaging over a timescale that is long compared to the timescale associated with fluctuations of the dynamo process but short compared to the evolutionary timescale of the core it is assumed that convection mixes the outer core to a basic state of hydrostatic equilibrium, uniform composition ( $\nabla c_X^l = 0$  where  $c_X^l$  is the mass concentration of light impurity  $X$  in the liquid), and an adiabatic temperature  $T_{\text{a}}(r)$ . Radial variation of thermodynamic properties are supposed to far exceed lateral variations (Stevenson, 1987) and so all variables are assumed to vary only in radius  $r$  with  $r_{\text{o}}$  the CMB and  $r_{\text{i}}(t)$  the ICB, which changes in time  $t$  as the inner core grows. These approximations are also taken to hold in the inner core. Although the

127 viability of inner core convection is currently the subject of debate (see Buffett, 2009; Pozzo  
 128 et al., 2014, for a discussion), Labrosse et al. (1997) suggest that this assumption has only a  
 129 minor effect on the results. With these approximations, the energy balance can be written  
 130 (Gubbins et al., 2003, 2004)

$$\begin{aligned}
 \underbrace{-\oint k\nabla T \cdot \mathbf{n}dS}_{Q_{\text{cmb}}} = & \underbrace{-\frac{C_p}{T_o} \int \rho T_a dV \frac{dT_o}{dt}}_{Q_s} \underbrace{-4\pi r_i^2 L \rho_i C_r \frac{dT_o}{dt}}_{Q_L} + \underbrace{\alpha_c \frac{Dc_X^l}{Dt} \int \rho \psi dV}_{Q_g} \\
 & + \underbrace{\int \alpha_T T_a \frac{DP}{Dt} dV}_{Q_P} + \underbrace{4\pi r_i^2 L \rho_i C_r \frac{dT_m}{dP} \frac{DP}{Dt}}_{Q_{PL}} + \underbrace{\int \rho h dV}_{Q_r},
 \end{aligned} \tag{1}$$

131 where

$$\frac{Dc_X^l}{Dt} = \frac{4\pi r_i^2 \rho_i}{M_{\text{oc}}} C_r (c_X^l - c_X^s) \frac{dT_o}{dt} \tag{2}$$

132 and

$$C_r = \frac{1}{(dT_m/dP)_{r=r_i} - (\partial T_a/\partial P)_{r=r_i}} \frac{1}{\rho_i g_i} \frac{T_i}{T_o}. \tag{3}$$

133 Here the density  $\rho(r)$ , gravity  $g(r)$ , gravitational potential  $\psi(r)$ , pressure  $P(r)$ , thermal  
 134 expansion coefficient  $\alpha_T$  and melting temperature  $T_m(r)$  are functions of  $r$  and subscripts  
 135 i and o refer to quantities evaluated at  $r_i$  and  $r_o$ , respectively. In writing equation (1) the  
 136 CMB has been assumed to be insulating, and the specific heat capacity at constant pressure  
 137  $C_p$ , compositional expansion coefficient  $\alpha_c = \rho^{-1}(\partial\rho/\partial c_X)_{P,T}$  and latent heat  $L$  have been  
 138 assumed constant. All other parameters are defined in Table 1. In writing equation (2) it  
 139 has been assumed that the concentration of element  $X$  in the solid,  $c_X^s$ , does not vary in  
 140 time. This is shown to be a good approximation in Figure 6 below. Note that  $Q_{\text{cmb}}$  contains  
 141 the total temperature  $T$  rather than the adiabatic temperature.  $\mathbf{n}$  is the outward normal to  
 142 the surface  $S$ , which encloses the volume  $V$  of the core;  $V_{\text{oc}}$  is the volume of the outer core.

143 Equation (1) states that the total CMB heat flow  $Q_{\text{cmb}}$  is balanced by heat released from  
 144 cooling the core  $Q_s$ , latent heat release due to the phase change at the ICB  $Q_L$ , gravitational  
 145 energy due to the segregation of light elements into the liquid phase on freezing  $Q_g$ , heat  
 146 released due to slow contraction of the core  $Q_P + Q_{PL}$  and radiogenic heating  $Q_r$ . It describes  
 147 the thermal evolution of the core but does not explicitly contain the magnetic field  $\mathbf{B}$  and  
 148 hence does not say anything about maintaining the geodynamo.  $\mathbf{B}$  does appear in the

149 entropy balance, which can be written (Gubbins et al., 2003, 2004)

$$\begin{aligned}
& \underbrace{\frac{1}{\mu_0^2} \int \frac{(\nabla \times \mathbf{B})^2}{T_a \sigma} dV}_{E_J} + \underbrace{\int k \left( \frac{\nabla T_a}{T_a} \right)^2 dV}_{E_k} + \underbrace{\alpha_c^2 \alpha_D \int \frac{g^2}{T_a} dV}_{E_a} \\
&= \underbrace{\frac{C_p}{T_o} \left( M_c - \frac{1}{T_o} \int \rho T_a dV \right)}_{E_s} \frac{dT_o}{dt} - \underbrace{Q_L \frac{(T_i - T_o)}{T_i T_o}}_{E_L} + \underbrace{\frac{Q_g}{T_o}}_{E_g} + \\
&\quad \underbrace{\frac{Q_P}{T_o} - \int \alpha_T \frac{DP}{Dt} dV}_{E_P} + \underbrace{Q_{PL} \left( \frac{1}{T_o} - \frac{1}{T_i} \right)}_{E_{PL}} + \\
&\quad \underbrace{h \left( \frac{M_c}{T_o} - \int \frac{\rho}{T_a} dV \right)}_{E_r} - \underbrace{\frac{Dc_X^l}{Dt} \int \rho \left( \frac{\partial \mu}{\partial T} \right)_{P,c} dV}_{E_h} \quad (4)
\end{aligned}$$

150 This equation shows that three positive definite sources of entropy, the Ohmic heating  $E_J$ ,  
151 entropy of thermal conduction  $E_k$ , and the entropy of molecular diffusion of light elements  
152  $E_a$ , balance entropy production associated with secular cooling  $E_s$ , gravitational energy  
153 release  $E_g$ , latent heat release  $E_L$ , contraction  $E_P + E_{PL}$ , radiogenic heating  $E_r$  and heat of  
154 reaction  $E_h$ . Here the viscous dissipation, which is supposed to be small in the core (Gubbins  
155 et al., 2003), has been neglected. Note that the definition of heat of reaction differs from  
156 that given in Gubbins et al. (2004); this issue was identified by F. Nimmo (pers comms).

157 Equations (1) and (4) can be written in the compact form (Gubbins et al., 2004; Nimmo,  
158 2007)

$$\begin{aligned}
Q_{\text{cmb}} &= \left( \tilde{Q}_s + \tilde{Q}_L + \tilde{Q}_g + \tilde{Q}_P + \tilde{Q}_{PL} \right) \frac{dT_o}{dt} + \tilde{Q}_r h, \\
E_J + E_k + E_a &= \left( \tilde{E}_s + \tilde{E}_L + \tilde{E}_g + \tilde{E}_P + \tilde{E}_{PL} + \tilde{E}_h \right) \frac{dT_o}{dt} + \tilde{E}_r h,
\end{aligned} \quad (5)$$

159 where  $Q_L = \tilde{Q}_L (dT_o/dt)$  and similarly for other terms. The tilde quantities can be calculated  
160 using knowledge of the radial variation of core properties. Equations (5) show that knowledge  
161 of the CMB heat-flux  $Q_{\text{cmb}}$  and the amount of radiogenic heat production per unit mass  $h$   
162 determines the cooling rate of the core  $dT_o/dt$  and hence the Ohmic heating  $E_J$ .  $E_J$  can  
163 be related to the gravitational energy that drives convective motion (Buffett et al., 1996)  
164 and hence represents the fraction of the input energy that ends up doing useful work by  
165 generating magnetic field.  $dT_o/dt$  is also related to the growth rate of the inner core,  $dr_i/dt$ ,  
166 by (Gubbins et al., 2003)

$$\frac{dr_i}{dt} = C_r \frac{dT_o}{dt}. \quad (6)$$

167 Equally, specifying  $E_J$  and  $h$  determines  $dT_o/dt$  and  $Q_{\text{cmb}}$ . Owing to the significant uncer-  
168 tainties in  $E_J$  and  $Q_{\text{cmb}}$ , both approaches are considered in this work.

169 It should be noted that equations (1) and (4) do not explicitly contain the fluid velocity.  
 170 The fact that the core is vigorously convecting is implicit in the formulation because it is  
 171 assumed that this convection maintains an adiabatic and compositionally uniform state when  
 172 short timescale phenomena are averaged out. The main product of the geodynamo process,  
 173  $\mathbf{B}$ , appears in the entropy balance although it does not need to be evaluated explicitly  
 174 because determining  $E_J$  is enough to assess the viability of dynamo action. Therefore,  
 175 equations (5) allow the long-term evolution of the core to be determined without requiring  
 176 detailed knowledge of the fluid flow or magnetic field.

177 The following sections describe the expressions used to evaluate the integrals in equations  
 178 (1) and (4) and the model of core chemistry. The term “core structure” is used to refer to  
 179 the radial variation of core properties.

### 180 2.1. Core structure

181 The radial variation of  $\rho(r)$ ,  $g(r)$ ,  $\psi(r)$ ,  $P(r)$ ,  $T_m(r)$ ,  $T_a(r)$  and  $k(r)$  is approximated by  
 182 polynomials, which allows the integrals in equations (1) and (4) to be written analytically.  
 183 The form of the expressions is chosen primarily to fit observational data rather than from  
 184 theoretical considerations. Present-day core structure is now fairly well-known. Unfortu-  
 185 nately, information on past core structure is almost non-existent. Cooling on the adiabat is  
 186 independent of position to a good approximation (Gubbins et al., 2003), suggesting that past  
 187 and present adiabatic profiles will be similar. Indeed, the cooling contribution to other fields  
 188 (density, etc) should also not significantly affect the time variation of their radial profiles.  
 189 Contraction could change the radial variation of core properties, but these effects are small  
 190 for the present-day (Gubbins et al., 2003) and are shown below to make a small contribution  
 191 to the long-term core evolution. We therefore take the view that obtaining a good fit to  
 192 present-day core structure is of particular importance. Alternative expressions for radial  
 193 core structure have been used in previous studies (e.g. Labrosse et al., 1997; Nimmo, 2014)  
 194 and these will be discussed in section 3.

#### 195 2.1.1. Density

196 Core density is taken from the Preliminary Reference Earth Model (PREM) (Dziewonski  
 197 and Anderson, 1981). Dziewonski and Anderson (1981) give a polynomial fit to the PREM  
 198 density data, which can be written as

$$\begin{aligned} \rho(r) &= \rho_0^{\text{ic}} + \rho_2^{\text{ic}} r^2 & 0 \leq r \leq r_i, \\ &= \rho_0^{\text{oc}} + \rho_1^{\text{oc}} r + \rho_2^{\text{oc}} r^2 + \rho_3^{\text{oc}} r^3 & r_i \leq r \leq r_o, \end{aligned} \quad (7)$$

199 where the  $\rho_i^{\text{oc}}$  are coefficients evaluated from a least squares fit of (7) to the outer core  
 200 PREM density data and  $\rho_i^{\text{ic}}$  are similar coefficients for the inner core. This expression for  $\rho$   
 201 accounts for the density jump at the ICB.

202 With this definition of  $\rho$  the mass of the inner core is

$$M_{\text{ic}} = 4\pi \int_0^{r_i} \rho r^2 dr = 4\pi \left[ \frac{\rho_0^{\text{ic}} r_i^3}{3} + \frac{\rho_2^{\text{ic}} r_i^5}{5} \right] \quad (8)$$



203 and the mass of the outer core is

$$\begin{aligned}
M_{\text{oc}} &= 4\pi \int_{r_i}^{r_o} \rho r^2 dr \\
&= 4\pi \left[ \frac{\rho_0^{\text{oc}} r_o^3}{3} + \frac{\rho_1^{\text{oc}} r_o^4}{4} + \frac{\rho_2^{\text{oc}} r_o^5}{5} + \frac{\rho_3^{\text{oc}} r_o^6}{6} - \left( \frac{\rho_0^{\text{oc}} r_i^3}{3} + \frac{\rho_1^{\text{oc}} r_i^4}{4} + \frac{\rho_2^{\text{oc}} r_i^5}{5} + \frac{\rho_3^{\text{oc}} r_i^6}{6} \right) \right]. \quad (9)
\end{aligned}$$

204 The mass of the whole core  $M_c = M_{\text{ic}} + M_{\text{oc}}$ . The variation of gravity  $g$  across the inner  
205 core is given by

$$g(r) = \frac{4\pi G}{r^2} \int_0^r \rho r'^2 dr' = 4\pi G \left[ \frac{\rho_0^{\text{ic}} r}{3} + \frac{\rho_2^{\text{ic}} r^3}{5} \right] \quad 0 \leq r \leq r_i. \quad (10)$$

206 Denoting  $g(r_i)$  by  $g_i^-$  in equation (10) the variation of  $g$  across the outer core is

$$g(r) = 4\pi G \left( \frac{\rho_0^{\text{oc}} r}{3} + \frac{\rho_1^{\text{oc}} r^2}{4} + \frac{\rho_2^{\text{oc}} r^3}{5} + \frac{\rho_3^{\text{oc}} r^4}{6} - \left[ \frac{\rho_0^{\text{oc}} r_i^3}{3r^2} + \frac{\rho_1^{\text{oc}} r_i^4}{4r^2} + \frac{\rho_2^{\text{oc}} r_i^5}{5r^2} + \frac{\rho_3^{\text{oc}} r_i^6}{6r^2} \right] \right) + \left( \frac{r_i^2}{r^2} \right) g_i^-. \quad (11)$$

207 Equations (10) and (11) preserve continuity of  $g$  across the ICB.

208 The variation of the gravitational potential across the outer core is needed to evaluate  
209 the  $Q_g$  terms in equations (5). Relative to zero potential at the CMB it is

$$\begin{aligned}
\psi(r) = - \int_r^{r_o} g dr' &= 4\pi G \left( \left[ \frac{\rho_0^{\text{oc}} r^2}{6} + \frac{\rho_1^{\text{oc}} r^3}{12} + \frac{\rho_2^{\text{oc}} r^4}{20} + \frac{\rho_3^{\text{oc}} r^5}{30} \right]_{r_o}^r - \right. \\
&\quad \left. \left[ \frac{\rho_0^{\text{ic}} r_i^3}{3r} + \frac{\rho_2^{\text{ic}} r_i^5}{5r} \right]_{r_o}^r + \left[ \frac{\rho_0^{\text{oc}} r_i^3}{3r} + \frac{\rho_1^{\text{oc}} r_i^4}{4r} + \frac{\rho_2^{\text{oc}} r_i^5}{5r} + \frac{\rho_3^{\text{oc}} r_i^6}{6r} \right]_{r_o}^r \right). \quad (12)
\end{aligned}$$

210 In both equations (11) and (12) the second and third terms in square brackets arise  
211 from the ICB density jump. These terms make a maximum contribution of 2% to the value  
212 of  $g(r)$  and 0.5% to  $\psi(r)$ , as shown in Figure 1. The gravity profile is needed to obtain  
213 the pressure, but neglecting the contribution from the density jump gives a  $P(r)$  [equation  
214 (13)] that differs by at most 1% from the PREM pressure.  $g(r_i)$  is needed in equation (3);  
215 however, as  $g$  is continuous across the ICB,  $g(r_i)$  can also be obtained from equation (10),  
216 which matches PREM to within a fraction of a percent. The gravitational potential profile  
217 is needed to evaluate  $Q_g$ , but neglecting the contribution to  $\psi(r)$  from the density jump  
218 gives an answer that is very close to previous studies (section 3). We therefore neglect the  
219 contributions to  $g(r)$  and  $\psi(r)$  from the ICB density jump and use the profiles shown by  
220 solid lines in Figure 1.

221 The pressure variation is obtained from the hydrostatic equation. Across the inner core

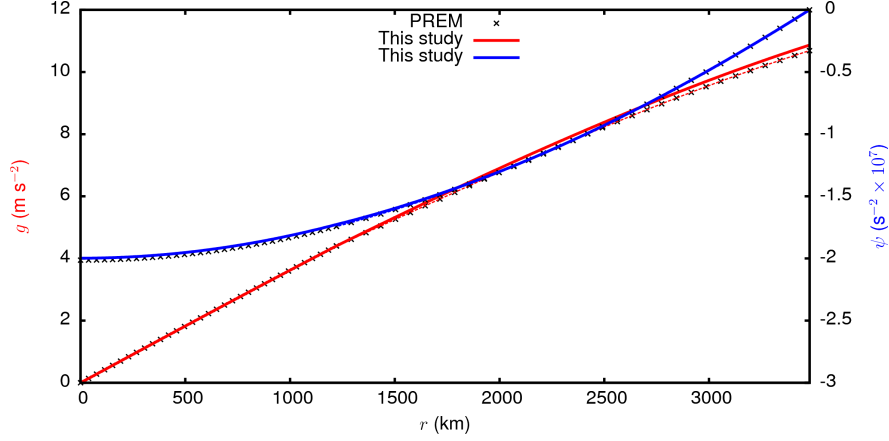


Figure 1: Radial variation of gravity  $g$  (left ordinate) and gravitational potential  $\psi$  (right ordinate). Crosses denote  $g$  and  $\psi$  obtained from PREM. Dashed lines show the polynomial expressions in equations (10), (11) and (12); solid lines use these equations but omitting the terms that arise from the ICB density jump.

222 it is given by

$$\begin{aligned}
 P(r) = \int_r^{r_o} \rho g dr' = -4\pi G \left[ \frac{\rho_0^{\text{oc}2}}{6} r^2 + \frac{7\rho_0^{\text{oc}} \rho_1^{\text{oc}}}{36} r^3 + \left( \frac{2\rho_0^{\text{oc}} \rho_2^{\text{oc}}}{15} + \frac{\rho_1^{\text{oc}2}}{16} \right) r^4 + \right. \\
 \left. \left( \frac{\rho_0^{\text{oc}} \rho_3^{\text{oc}}}{10} + \frac{9\rho_1^{\text{oc}} \rho_2^{\text{oc}}}{100} \right) r^5 + \left( \frac{5\rho_1^{\text{oc}} \rho_3^{\text{oc}}}{72} + \frac{\rho_2^{\text{oc}2}}{30} \right) r^6 + \frac{11\rho_2^{\text{oc}} \rho_3^{\text{oc}}}{210} r^7 + \frac{\rho_3^{\text{oc}2}}{42} r^8 \right]_{r_i}^{r_o} \quad (13) \\
 + P_o - 4\pi G \left[ \frac{\rho_0^{\text{ic}2}}{6} r^2 + \frac{2\rho_0^{\text{ic}} \rho_2^{\text{ic}}}{15} r^4 + \frac{\rho_2^{\text{ic}2}}{30} r^6 \right]_r^{r_i},
 \end{aligned}$$

223 where  $P_o$  is the pressure at the CMB. The pressure variation across the outer core is obtained  
 224 by setting the term in the second square bracket to zero and putting  $r$  instead of  $r_i$  in the  
 225 lower limit of the term in the first square bracket.

### 226 2.1.2. Temperature

227 The adiabatic temperature satisfies the equation

$$T_a(r) = T_{\text{cen}} \exp \left( - \int_0^r \frac{g\gamma}{\phi} dr \right), \quad (14)$$

228 where  $T_{\text{cen}}$  is the temperature at the centre of the Earth,  $\gamma$  is the Grüneisen parameter and  
 229  $\phi$  is the seismic parameter. Here we approximate equation (14) by the polynomial

$$T_a(r) = T_{\text{cen}}(1 + t_1 r + t_2 r^2 + t_3 r^3). \quad (15)$$

230 Values for the coefficients  $t_i$  are obtained from a least-squares fit to equation (14) using  
 231  $\gamma \approx 1.5$  independent of radius (e.g. Gubbins et al., 2003; Stacey, 2007) and  $\phi$  and  $g$  from

232 PREM. The coefficient  $T_{\text{cen}}$  is set by the requirement that  $T_a$  equals the melting temperature  
 233 of the core mixture at the ICB.

234 We use the melting point data for pure iron from Alfè et al. (2002c). These data are fit  
 235 with a polynomial of the form

$$T_{\text{m,Fe}}(P) = t_{\text{m0}}(1 + t_{\text{m1}}P + t_{\text{m2}}P^2 + t_{\text{m3}}P^3), \quad (16)$$

236 where values for the coefficients  $t_{\text{mi}}$  are found from a least squares fit to the melting point  
 237 data.

238 The entropy of melting for pure iron  $\Delta S_{\text{Fe}}$  is written as

$$\Delta S_{\text{Fe}}(P) = S_1 + S_2P + S_3P^2 + S_4P^3, \quad (17)$$

239 where the coefficients  $S_i$  are obtained by fitting equation (17) to the data of Alfè et al.  
 240 (2002c). Note that the data of Alfè et al. (2002c) is given in units of the Boltzmann constant  
 241 and so equation (17) is also written in these units.  $\Delta S_{\text{Fe}}$  is used to determine the depression  
 242 of the melting point by light impurities below.

### 243 *2.1.3. Core chemistry*

244 The ICB density jump,  $\Delta\rho$ , arises partly because solid core material is denser than liquid  
 245 core material at the same pressure-temperature conditions and partly because the outer core  
 246 is enriched in light elements compared to the inner core (Poirier, 1994). The ICB density  
 247 jump therefore determines the relative importance of compositional and thermal convection  
 248 and is a crucial input parameter. Unfortunately  $\Delta\rho$  is uncertain by about 25%. Moreover,  
 249 although geochemical constraints are available, the actual elements are very poorly known  
 250 (see Nimmo, 2007, for a discussion) and so a candidate model of core chemistry must specify  
 251 the elements as well as their abundances subject to the constraints that the model density  
 252 profile matches the observed core density profile, including the jump at the ICB, together  
 253 with the mass of the core.

254 This study utilises two models of core chemistry (Alfè et al., 2002b, 2007) that satisfy  
 255 the constraints stated above. The first, hereafter labelled model PREM, has  $\Delta\rho = 0.6 \text{ g cm}^{-1}$   
 256 (Dziewonski and Anderson, 1981); it consists of an iron inner core with 10% S and/or  
 257 Si and an outer core with 8.5% S and/or Si plus an additional 8% O. The second, hereafter  
 258 labelled model MG, has  $\Delta\rho = 0.8 \text{ g cm}^{-1}$  (Masters and Gubbins, 2003); it consists of an iron  
 259 inner core with 8% S and/or Si and an outer core with the same mixture plus an additional  
 260 13% O. Alfè et al. (2002b) find that S and Si partition almost equally between the inner  
 261 and outer cores, while O partitions almost entirely into the liquid; it is therefore O that is  
 262 mainly responsible for the compositional part of the ICB density jump in these models. The  
 263 contributions of all three elements to the gravitational terms  $Q_g$  and  $E_g$  and to the entropy  
 264 of molecular diffusion  $E_a$  are calculated separately and combined by simple addition.

265 The presence of a light element  $X$  in the core depresses the melting temperature of pure  
 266 iron by an amount  $\Delta T_X$ . The intersection of the melting curve and the adiabat determines  
 267 the ICB radius and so the melting point depression is an important parameter.  $\Delta T_X$  depends  
 268 on the concentration of  $X$  in the liquid and solid. Gubbins et al. (2013) showed how to obtain

269 the solid concentration from the liquid concentration for O, and (Labrosse, 2014) performed  
 270 the calculation for S. Here we extend this work to calculate the partitioning of Si and  
 271 use these results to obtain the melting point depression due to O, S and Si. As in Labrosse  
 272 (2014) and Alfè et al. (2002b) we assume that the concentrations of the various species evolve  
 273 independently of each other. It is convenient to use molar rather than mass concentrations,  
 274 which will be denoted by an overbar. The equations needed to convert between molar and  
 275 mass concentrations are given by Labrosse (2014).

276 According to the theory of Alfè et al. (2002a),  $\Delta T_X^m$  is given by

$$\Delta T_X = \frac{T_{m,Fe}}{\Delta S_{Fe}} (\bar{c}_X^s - \bar{c}_X^l). \quad (18)$$

277 An equation for  $\bar{c}_X^s$  can be obtained from the condition for thermodynamic equilibrium at  
 278 the ICB, which requires that the chemical potentials of the solid and liquid be equal (Alfè  
 279 et al., 2002a). This condition can be written

$$\mu_0^l + \lambda^l \bar{c}_X^l + k_B T_m \ln \bar{c}_X^l = \mu_0^s + \lambda^s \bar{c}_X^s + k_B T_m \ln \bar{c}_X^s, \quad (19)$$

280 where  $\mu_0^l$  and  $\mu_0^s$  are the (constant) chemical potentials for the liquid and solid re-  
 281 spectively,  $\lambda^l$  and  $\lambda^s$  are constants representing corrections to the  $\mu_0$  terms (Alfè et al.,  
 282 2002a), and  $k_B$  is Boltzmann's constant. Assuming that each light element makes an in-  
 283 dependent contribution to the melting temperature  $T_m$  of the mixture we can substitute  
 284  $T_m = T_{m,Fe} + \Delta T_X$  into equation (19) and obtain a transcendental equation that must be  
 285 solved for  $\bar{c}_X^s$ :

$$\Delta \mu_0 + \lambda^l \bar{c}_X^l - \lambda^s \bar{c}_X^s - k_B T_{m,Fe} \ln \left( \frac{\bar{c}_X^s}{\bar{c}_X^l} \right) \left( 1 + \frac{(\bar{c}_X^s - \bar{c}_X^l)}{\Delta S_{Fe}} \right) = 0, \quad (20)$$

286 where  $\Delta \mu_0 = \mu_0^l - \mu_0^s$ . For an initial value of  $\bar{c}_X^l$  this equation is solved by the bisection  
 287 method for each species, O, S and Si. The depression of the melting point for each species  
 288 is then obtained from equation (18). Finally, the melting temperature of the mixture,  $T_m$ ,  
 289 is calculated according to

$$T_m = T_{m,Fe} + \sum_i \Delta T_i, \quad (21)$$

290 where the sum is over O, S, and Si and  $T_{m,Fe}$  is given by equation (16). The liquid  
 291 concentration evolves in time according to equation (2), which provides the value of  $\bar{c}_X^l$  at  
 292 each time point and the procedure is repeated.

293 The radial variation of thermal conductivity is parametrised by

$$k(r) = k_0 + k_1 r + k_2 r^2. \quad (22)$$

294 where  $k_0$ ,  $k_1$  and  $k_2$  are coefficients that are obtained by fitting (22) to the data of Pozzo  
 295 et al. (2013). This expression ignores the jump in  $k$  at the ICB (Pozzo et al., 2014), but this  
 296 will cause only a slight change in the value of  $E_k$ .

297 The derivatives  $(\frac{\partial\mu}{\partial c})_{P,T}$  and  $(\frac{\partial\mu}{\partial T})_{P,c}$  of the chemical potential for O and Si are computed  
298 using the data of Alfè et al. (2002a) (see Gubbins et al. (2004) for details of the calculations).  
299 The quantity  $\alpha_D = \rho D / (\frac{\partial\mu}{\partial c})_{P,T}$ , which arises in the entropy of molecular diffusion  $E_a$ , also  
300 depends on the mass diffusion coefficients  $D$  for O and Si. Pozzo et al. (2013) found that  
301  $D$  varies with depth for O, S, and Si, but this variation is unimportant for the calculations  
302 here because  $E_a$  is small and so we use constant  $D$ . The expansion coefficients  $\alpha_c$  for O, S  
303 and Si are taken from Gubbins et al. (2004).

| Symbol  | Definition                        | Units                            | This Study | N14    | P12    |        |
|---|-----------------------------------|----------------------------------|------------|--------|--------|--------|
| $T_a$   | Temperature                       | K                                |            |        |        |        |
| $T_m$   | Melting temperature               | K                                |            |        |        |        |
| $g$   | Gravity                           | $\text{m s}^{-2}$                |            |        |        |        |
| $\psi$  | Gravitational potential           | $\text{s}^{-2}$                  |            |        |        |        |
| $P$   | Pressure                          | Pa                               |            |        |        |        |
| $\rho$  | Density                           | $\text{kg m}^{-3}$               |            |        |        |        |
| $\mathbf{B}$                                  | Magnetic field intensity          | T                                |            |        |        |        |
| $\sigma$                                      | Electrical conductivity           | $\text{S m}^{-1}$                |            |        |        |        |
| $k$   | Thermal conductivity              | $\text{W m}^{-1}\text{K}^{-1}$   |            |        |        |        |
| $\mu$   | Chemical potential                | $\text{J mol}^{-1}$              |            |        |        |        |
| $\Delta\rho$                                  | ICB density jump                  | $\text{g cc}^{-1}$               | 0.6, 0.8   | 0.8    | 0.8    |        |
| $\frac{dT_o}{dt}$                             | CMB cooling rate                  | $\text{K Gyr}^{-1}$              |            |        |        |        |
| $h$   | Radiogenic heating by mass        | $\text{W kg}^{-1}$               |            |        |        |        |
| $Q_{\text{cmb}}$                              | Total CMB heat-flux               | W                                |            |        |        |        |
| $E_J$   | Ohmic heating                     | $\text{W K}^{-1}$                |            |        |        |        |
| $C_p$   | Specific heat (constant pressure) | $\text{J kg}^{-1} \text{K}^{-1}$ | 715        | 840    | 715    |        |
| $L$   | Latent heat of freezing           | $\text{MJ kg}^{-1}$              | 0.75       | 0.75   | 0.75   |        |
| $\alpha_T$                                    | Thermal expansion coefficient     | $\text{K}^{-1} \times 10^{-5}$   | 1.35       | 1.25   |        |        |
| $\mu_0$                                       | Permeability of free space        | $\text{H m}^{-1} \times 10^{-7}$ | $4\pi$     | $4\pi$ | $4\pi$ |        |
| $r_o$   | Outer core radius                 | km                               | 3480       | 3480   | 3480   |        |
| $r_i$   | Inner core radius                 | km                               | 1221       | 1220   | 1221   |        |
| $M_c$   | Mass of core                      | $\text{kg} \times 10^{24}$       | 1.94       | 1.93   | 1.9477 |        |
| $M_{oc}$                                      | Mass of outer core                | $\text{kg} \times 10^{24}$       | 1.84       | 1.83   | 1.85   |        |
| $g_i$   | ICB gravity                       | $\text{m s}^{-2}$                | 4.40       | 4.23   | 4.40   |        |
| $\rho_i$                                      | ICB density                       | $\text{Mg m}^{-3}$               | 12.2       | 12.1   | 12.17  |        |
| $\frac{\partial T_m}{\partial P} \Big _{r_i}$ |                                   | $\text{K Gpa}^{-1}$              | 9.01       | 9.36   | 9.0    |        |
|   |                                   |                                  | PREM       | MG     | MG     | MG     |
| $k_o$   | CMB thermal conductivity          | $\text{W m}^{-1} \text{K}^{-1}$  | 107        | 99     | 130    | 100    |
| $T_i$   | ICB temperature                   | K                                | 5789       | 5497   | 5508   | 5500   |
| $T_o$   | CMB temperature                   | K                                | 4256       | 4046   | 4180   | 4039   |
| $c_O^l$                                       | Liquid O Concentration            |                                  | 0.0256     | 0.0428 | 0.0409 | 0.0428 |
| $c_S^l$                                       | Liquid S Concentration            |                                  | 0.0319     | 0.0263 | -      | -      |
| $c_{Si}^l$                                    | Liquid Si Concentration           |                                  | 0.0279     | 0.0230 | -      | 0.0461 |
| $\frac{\partial T_a}{\partial P} \Big _{r_i}$ |                                   | $\text{K Gpa}^{-1}$              | 6.57       | 6.24   | 6.86   | 6.32   |

|       |  |                   |        |       |        |       |
|-------|--|-------------------|--------|-------|--------|-------|
| $C_r$ |  | m K <sup>-1</sup> | -10559 | -9249 | -10220 | -9498 |
|-------|--|-------------------|--------|-------|--------|-------|

Table 1: Mathematical quantities used in the paper and, where relevant, the numerical values used in the calculations. Quantities in the third section are constant in time. Values in the fourth section are given for the present day; they are determined from the radial core structure. Quantities in the fifth section depend on the density jump at the inner core boundary (ICB). PREM refers to the model with ICB density jump  $\Delta\rho = 0.6$  g cc<sup>-1</sup> (Dziewonski and Anderson, 1981) and MG refers to the model with ICB density jump  $\Delta\rho = 0.8$  g cc<sup>-1</sup> (Masters and Gubbins, 2003).

## 304 2.2. Parameter Selection and Model setup

305 The expressions given in sections 2.1.1, 2.1.2 and 2.1.3 allow each of the integrals in  
306 equations (5) to be evaluated analytically. The calculations are straightforward but tedious;  
307 the results are given in the Appendix. Example profiles of  $\rho$ ,  $T_a$ ,  $T_m$  and  $k$  are shown in  
308 Figure 2 and discussed in more detail in the following section.

309 Equations (5) are evolved backwards in time from the present-day for a period of 3.5  
310 billion years using a timestep of 1 Myr, which is sufficient to resolve the rapid changes that  
311 arise around the time of inner core nucleation. The location of the ICB is found from the  
312 intersection of  $T_a$  and  $T_m$  at each timestep. Near the centre of the Earth  $T_a$  and  $T_m$  are  
313 almost parallel and so a small change in core temperature can change the predicted ICB  
314 radius from a few tens of km to a few metres; the inner core apparently “disappears”. It  
315 is also possible for  $T_a$  to cross  $T_m$  twice, i.e. a transition from liquid to solid to liquid.  
316 Such spurious behaviour is avoided by ensuring that  $dT_a/dr$  obtained from equation (15) is  
317 shallower than the melting gradient in the innermost few km. This is easily achieved while  
318 fitting the coefficients in equation (15) to within the least squares errors. The procedure  
319 favours older inner core ages as it takes more time to raise the core adiabat above  $T_m$  at  
320 all radii.

321 At the start of the calculation the coefficient  $T_{cen}$  that anchors the adiabat temperature  
322 [equation (15)] is set such that  $T_a$  is equal to the melting temperature at the present ICB  
323 radius,  $r_i = 1221$  km. Subsequently, the CMB temperature is updated from the calculated  
324 value of  $dT_o/dt$  and this is used to calculate a new adiabat with a new value of  $T_{cen}$ .

325 Liquid concentrations are evolved using equation (2). This is used to calculate a new  
326 melting curve that, together with the updated adiabat, define the new ICB radius. The  
327 core density (and hence gravity and pressure) may vary over time as the concentration  
328 changes, but this effect has been omitted as it was in previous studies (see Nimmo, 2014,  
329 for a review). We expect the effect to be minor because the concentration changes are very  
330 small (as demonstrated below), while the density decrease due to increasing light element  
331 concentration will be at least partially offset by a density increase as the core temperature  
332 falls. Also, we only account for changes in  $k(r)$  due to the density jump and do not model

333 the effect of time-varying concentration. The melting temperature, and hence the adiabatic  
334 temperature, do depend on temporal changes in light element concentration and so the  
335 coefficients  $\tilde{E}$  and  $\tilde{Q}$  in equations (5) also change in time.

336 As discussed above, the lack of observational constraints on the time evolution of  $E_J$  and  
337  $Q_{\text{cmb}}$  mean they are effectively unknowns for the purpose of this study. To proceed we must  
338 fix one to determine the other. For the purpose of constructing minimum bound models it  
339 is clearly sufficient to take  $Q_{\text{cmb}} = \text{constant}$  or  $E_J = \text{constant}$  such that the minimum value  
340 of  $E_J$  in the past 3.5 Ga is  $\geq 0$ .

341 Mantle convection simulations (e.g. Nakagawa and Tackley, 2013, 2014) and models of  
342 mantle thermal history (e.g. Jaupart et al., 2007) predict significant variations in  $Q_{\text{cmb}}$  with  
343 time and so we do not consider the case  $Q_{\text{cmb}} = \text{constant}$ . The simplest option, considered  
344 in section 4.1, is to set  $E_J = 0$ , which gives the minimum allowable cooling rate (recall that  
345  $E_J$  must be positive) and hence the oldest inner core and coolest ancient core temperature.  
346 However, this case produces an unrealistically sharp increase in  $Q_{\text{cmb}}$  at the time of inner core  
347 formation (Labrosse, 2003) and is therefore purely illustrative. Nimmo (2007) suggests fixing  
348  $E_J = \text{constant}$  before inner core nucleation and  $Q_{\text{cmb}} = \text{constant}$  during inner core growth.  
349 This prescription has the advantage of producing the basic shape of  $Q_{\text{cmb}}(t)$  obtained in some  
350 mantle convection simulations (e.g. Nakagawa and Tackley, 2013, 2014) and is considered in  
351 section 4.2.

352 Parameter values used in this study are listed in column 4 of Table 1. Unless otherwise  
353 stated they are taken from the previous studies of Pozzo et al. (2012) and Pozzo et al. (2013).  
354 Parameter values used by Nimmo (2014) are listed in column 5 of Table 1. Parameter values  
355 used by Pozzo et al. (2012) are listed in column 6 of Table 1. The effects of different choices  
356 will be assessed in section 3. Parameters in the third section of Table 1 are taken to be  
357 constant in radius and time. Although  $\alpha_T$  varies by a factor of two across the core (Gubbins  
358 et al., 2003), it only enters in the small terms associated with contraction and can safely be  
359 taken as constant without affecting the results; accounting for the variation of  $\alpha_T$  requires  
360 a numerical solution that shows the contraction terms remain small (Gubbins et al., 2003).  
361 Parameters in the fourth section of Table 1 are derived from the radial profiles developed in  
362 the previous section. Parameters in the final section depend on the ICB density jump and  
363 core chemistry.

364 The most uncertain model input parameters are the ICB density jump  $\Delta\rho$ , the thermal  
365 conductivity, and the amount of radiogenic heat production  $h$ . Masters and Gubbins (2003)  
366 conclude that  $\Delta\rho = 0.8 \pm 0.2 \text{ gm cc}^{-1}$ . Here we consider the two values  $\Delta\rho = 0.6$  (denoted  
367 model PREM) and  $\Delta\rho = 0.8 \text{ gm cc}^{-1}$  (denoted model MG) as described in section 2.1.3.  
368 Alfè et al. (2002b) do not distinguish between the behaviour of S and Si so for simplicity we  
369 assume they are present in equal (molar) amounts, i.e. 5% of both S and Si in the liquid  
370 for model PREM and 4% of both S and Si in the liquid for model MG. Solid concentrations  
371 are calculated from liquid concentrations as described in section 2.1.3 using the parameters  
372 listed in Table 2, which are taken from Alfè et al. (2002b) and Gubbins et al. (2013).

373 The thermal conductivity also depends on the nature and amount of impurity. Differences  
374 in recent estimates of  $k_o = k(r_o) = 80\text{--}110 \text{ W m}^{-1} \text{ K}^{-1}$  (de Koker et al., 2012; Pozzo et al.,  
375 2013; Gomi et al., 2013), and also in the radial variation of  $k$ , are in large part due to the

| Symbol  | Definition                     | Units  | O      | S     | Si    |
|---|--------------------------------|--|--------|-------|-------|
| $\bar{c}_X^s$ (PREM)                                | Solid concentration            |  | 0.0002 | 0.022 | 0.026 |
| $\bar{c}_X^s$ (MG)                                  | Solid concentration            |  | 0.0004 | 0.017 | 0.020 |
| $\Delta\mu_0$                                       | $\mu_0^l - \mu_0^s$            | eV/atom  | -2.6   | -0.25 | -0.05 |
| $\lambda_X^s$                                       | Correction, solid              |  | 0.0    | 5.9   | 2.7   |
| $\lambda_X^l$                                       | Correction, liquid             |  | 3.25   | 6.15  | 3.6   |
| $\alpha_c$  | Chemical expansion coefficient |  | 1.1    | 0.64  | 0.87  |
| $D$   | Mass diffusivity               | $\text{m}^2 \text{s}^{-1} \times 10^{-8}$        | 1      | 0.5   | 0.5   |
| $\alpha_D$  | Coefficient                    | $\text{kg m}^{-3} \text{s} \times 10^{-12}$      | 0.70   | 0.81  | 0.75  |
| $\left(\frac{\partial\mu}{\partial T}\right)_{P,c}$ | CMB value                      | $\text{J mol}^{-1} \text{K}^{-1} \times 10^{-4}$ | -4.5   | -     | 1.1   |
| $\left(\frac{\partial\mu}{\partial T}\right)_{P,c}$ | Centre of Earth value          | $\text{J mol}^{-1} \text{K}^{-1} \times 10^{-4}$ | -2.3   | -     | 1.9   |

Table 2: Parameters that define the model of core chemistry used in this study. Solid concentrations are given for the present-day.

376 use of different core compositions. Here we take a simple approach to account for these  
377 differences in  $k$  by using the two radial profiles of Pozzo et al. (2013) shown in Figure 2 and  
378 changing  $k_o$ . For model PREM, Pozzo et al. (2013) find  $k_o = 107 \text{ W m}^{-1} \text{ K}^{-1}$  so we take  
379  $k_o = 100, 107$  and  $115 \text{ W m}^{-1} \text{ K}^{-1}$  as representative of the variation. For model MG, Pozzo  
380 et al. (2013) find  $k_o = 99 \text{ W m}^{-1} \text{ K}^{-1}$  and so we take  $k_o = 90, 99$  and  $110 \text{ W m}^{-1} \text{ K}^{-1}$ .

381 The amount of radiogenic heat production in the core is still highly uncertain (Nimmo,  
382 2007). To compare to previous studies that incorporate radiogenic heating we consider  
383 potassium (Nimmo et al., 2004). The amount of radiogenic heat production  $h$  is evolved  
384 backwards in time via the equation

$$h = h_0 2^{t/t_{1/2}}, \quad (23)$$

385 where  $t_{1/2} = 1.248 \text{ Gyr}$  is the half-life of  $^{40}\text{K}$  and  $h_0$  is the present day heat production due to  
386  $^{40}\text{K}$ . The time variation produces a factor of 7 variation in  $h$  over 3.5 Ga. To compare with  
387 the results of Nimmo (2014) we consider  $h_0 = 0$  and  $h_0 = 300 \text{ ppm}$ . The latter is probably  
388 higher than is acceptable on geochemical grounds and represents an extreme scenario.

### 389 3. Comparison with previous models

390 Previous studies (Buffett et al., 1996; Labrosse et al., 1997; Nimmo, 2014) have adopted  
391 different parameter values and analytical expressions for radial core structure from those  
392 used here. To demonstrate the influence of the different choices we compare the model  
393 developed in section 2.1, here labelled POLY, to that used by Pozzo et al. (2012) (hereafter  
394 P12) and Nimmo (2014) (hereafter N14). The parameter values used in P12 and N14 are  
395 presented in Table 1. P12 only calculated the present-day core energy budget, but did so  
396 by numerically integrating equations (5) using the data for  $T_a$ ,  $T_m$ , etc, obtained directly  
397 from seismic and mineralogical studies. Their present-day results serve as a benchmark with  
398 which to compare the POLY and N14 models. N14 calculated core thermal histories over



399 the last 4.5 Gyr. To do so he followed Labrosse et al. (1997) by writing the density, adiabatic  
 400 temperature, melting temperature and thermal conductivity as

$$\rho(r) = \rho_{\text{cen}} \exp^{-r^2/L^2}, \quad (24)$$

$$T_{\text{a}}(r) = T_{\text{cen}} \exp^{-r^2/D^2}, \quad (25)$$

$$T_{\text{m}}(r) = T_{m0}(1 + t_{m1}P + t_{m2}P^2), \quad (26)$$

$$k(r) = k(r_{\text{o}}) \frac{1 - \frac{r^2}{D_k^2}}{1 - \frac{r_{\text{o}}^2}{D_k^2}}, \quad (27)$$

401 where  $L \approx 7000$  km,  $D \approx 6000$  km and  $D_k$  are lengths defined in Nimmo (2014). These  
 402 profiles will be denoted N14 $\rho$ , N14 $T_{\text{a}}$ , N14 $T_{\text{m}}$  and N14 $k$ . Note that Nimmo (2014) used  
 403  $k = 130$  W m<sup>-1</sup>K<sup>-1</sup> independent of depth and so the same is done here. We first compare  
 404 the radial profiles used in the POLY and N14 models to P12, who used the PREM density  
 405 profile, the melting data of Alfè et al. (2002c) and equation (14) for  $T_{\text{a}}$  with  $\gamma = 1.5$ . We  
 406 then compare models based on a published solution for the present-day energy budget before  
 407 evolving this solution backwards in time using the POLY and N14 models.

408 Figure 2 compares the POLY and N14 radial profiles. The main difference between the  
 409 density profiles is that N14 $\rho$  does not account for the ICB density jump. The theoretical  
 410 adiabats and melting curves differ significantly at the top of the core. This difference be-  
 411 tween the melting curves is not important because  $T_{\text{m}}$  only enters the equations through  
 412  $dT_{\text{m}}/dr|_{r=r_1}$ . However, the difference in  $T_{\text{a}}$  at the top of the core is significant because  
 413  $\partial T_{\text{a}}/\partial r|_{r=r_{\text{o}}}$  is needed to determine the adiabatic heat-flux and hence the condition of neu-  
 414 tral stability. Using  $k(r_{\text{o}}) = 99$  W m<sup>-1</sup> K<sup>-1</sup> we find that  $Q_{\text{k}} = 14.8$  TW for the POLY  $T_{\text{a}}$   
 415 profile and  $Q_{\text{k}} = 11.5$  TW using the N14  $T_{\text{a}}$  profile, a significant difference. The profiles of  
 416  $T_{\text{m}}$  and  $T_{\text{a}}$  are similar in the lower half of the core, but it should be noted that the gravi-  
 417 tational energy and latent heat terms are very sensitive to small differences in  $dT_{\text{m}}/dP|_{r=r_1}$   
 418 and  $\partial T_{\text{a}}/\partial P|_{r=r_1}$ . Values for these gradients and the parameter  $C_r$  [equation (3)] at the  
 419 present day are given in Table 1 for the POLY, N14 and P12 models. The estimate of  $C_r$   
 420 using the POLY core structure is closest to the P12 value and differs by about 10% from  
 421 the value obtained with the N14 core structure. This difference affects the terms  $Q_{\text{L}}$ ,  $Q_{\text{PL}}$ ,  
 422  $Q_{\text{g}}$  and the associated entropy terms.

423 Table 3 lists individual terms in the energy and entropy balance at the present-day for  
 424 Case 5 of P12. This Case was chosen as it has also been reproduced by Nimmo (2014) (his  
 425 Table 4) using a different code. P12 neglected pressure heating and the heat of reaction and  
 426 this is also done here. In Table 3 the first part of each model name refers to the model of  
 427 core structure that is used (P12, POLY and N14) while the last two characters in each name  
 428 give the column number in Table 1 corresponding to the parameter values that are used.

429 Model POLYC4 calculates the melting behaviour as in section 2.1.3 and includes the  
 430 effect of S and Si in the gravitational energy. Model POLYC6 is designed to reproduce  
 431 the parameters adopted by P12. P12 set the ICB temperature to 5700 K; to mimic this  
 432 we prescribe a time-independent  $\Delta T_{\text{X}}$  in equation (21) such that  $T_{\text{m}}(r_1) = 5700$  K rather  
 433 than calculating it by the method described in section 2.1.3. The N14 models also use a

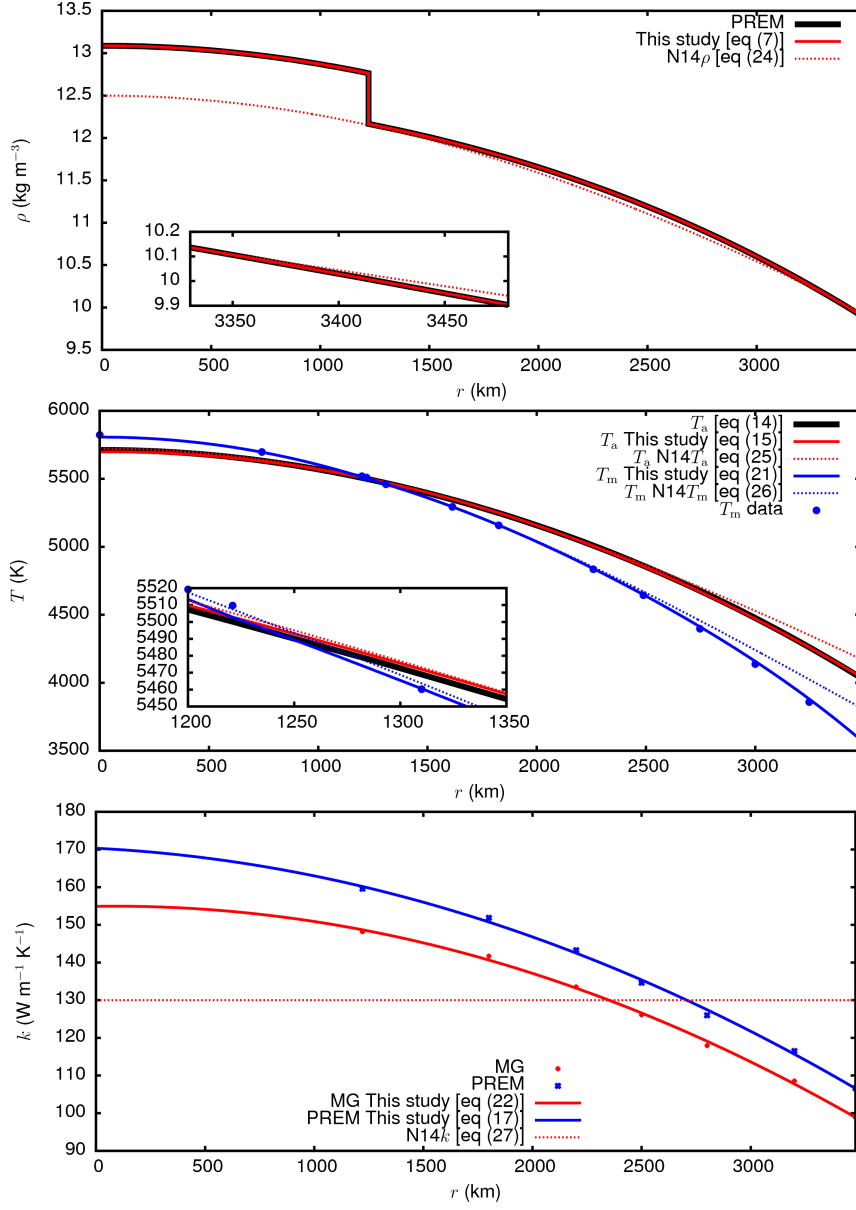


Figure 2: Top: radial variation of core density calculated from PREM (black line), Nimmo (2014) (red dashed line, equation (24)) and this study (red solid line, equation (7)). Inset shows a close-up of the profiles near the CMB. Middle: radial variation of the adiabatic temperature using equation (14) with  $g$  and  $\phi$  calculated from PREM (black), this study (equation (15), red solid line) and Nimmo (2014) (equation (25), red dashed line). Also shown are the melting data of Alfe et al. (2002c) (blue points), the melting curve from this study (equation (21), blue solid line) and the melting curve from Nimmo (2014) (equation (26), blue dashed line). Melting point data were linearly interpolated from pressure to radius. Bottom: radial variation of thermal conductivity  $k$  using data from Pozzo et al. (2013) (points), this study (equation (22), solid lines) and Nimmo (2014) (equation (27), dashed line). PREM refers to the density jump  $\Delta\rho = 0.6 \text{ g cc}^{-1}$  (Dziewonski and Anderson, 1981); MG refers to the density jump  $\Delta\rho = 0.8 \text{ g cc}^{-1}$  (Masters and Gubbins, 2003).

| Model  | $Q_s$ | $Q_L$ | $Q_g$ | $Q_k$ | $E_s$ | $E_L$ | $E_g$ | $E_a$ | $E_k$ | $E_J$ | $dT_o/dt$ | IC age |
|--------|-------|-------|-------|-------|-------|-------|-------|-------|-------|-------|-----------|--------|
| P12C6  | 5.93  | 5.92  | 3.35  | 15.2  | 212   | 389   | 830   | 5.81  | 561   | 865   | 115       | 373    |
| POLYC4 | 5.70  | 5.54  | 3.96  | 14.8  | 206   | 363   | 979   | 5.98  | 542   | 999   | 111       | 451    |
| POLYC6 | 5.90  | 5.77  | 3.54  | 14.8  | 213   | 377   | 874   | 5.98  | 542   | 901   | 115       | 455    |
| N14C5  | 6.01  | 5.78  | 3.41  | 14.9  | 181   | 333   | 816   | 0.0   | 451   | 877   | 102       | 500    |
| N14C6  | 5.38  | 6.13  | 3.70  | 11.5  | 162   | 351   | 885   | 0.0   | 346   | 1047  | 108       | 490    |

Table 3: Comparison of different parameterisations of core structure with Case 5 of Pozzo et al. (2012). Individual terms are defined in the text. All energy terms are in TW; entropy terms are in MW K<sup>-1</sup>;  $dT_o/dt$  in K Gyr<sup>-1</sup>; inner core (IC) age in Myr.  $Q_{\text{cmb}} = 15.2$  TW in all models. Model P12C6 corresponds to the results of Pozzo et al. (2012) and uses the parameters in column 6 (C6) of Table 1. Model POLYC4 uses the POLY core structure developed in section 2.1 and the parameters listed in column 4 (C4) of Table 1. Model POLYC6 uses the POLY core structure and is set up to reproduce the values in column 6 (C6) of Table 1. Model N14C5 is calculated using equations (24)–(27) for the Nimmo (2014) core structure and values for quantities given in Nimmo (2014) and column 5 of Table 1. Model N14C6 is calculated using equations (24)–(27) for Nimmo (2014) core structure and parameter values adopted in column 6 of Table 1. Pressure heating and heat of reaction have been neglected. All cases use model MG for core chemistry.

434 time-independent melting point depression. For model POLYC6 and the N14 models it is  
435 assumed, as in P12, that only O contributes to the gravitational energy and that all the O  
436 partitions into the liquid on freezing.

437 Table 1 shows that there is good agreement between the P12C6, POLYC6 and N14C5  
438 models. In particular, all terms in model POLYC6 are within  $\sim 5\%$  of the corresponding  
439 term for the P12C6 case. The POLYC4 model has more gravitational energy than model  
440 P12C6 because it accounts for contributions from S and Si; indeed, the contribution of O  
441 alone is 3.36 TW, very close to that of model P12. Model N14C5 is close to model P12C6  
442 but uses different values of  $C_p$  and  $k$  and so predicts a slower present-day cooling rate. There  
443 is weaker agreement between N14C6 and the other models.

444 Figure 3 shows the POLY and N14 models in Table 3 evolved backwards in time with  
445  $Q_{\text{cmb}}$  fixed during inner core growth and  $E_J$  fixed prior to inner core formation. This choice  
446 is made purely to illustrate the different model behaviour. Because the models are evolved  
447 backwards in time, the fixed value of  $E_J$  equals the value obtained at the first instant when  
448 there was no inner core. The difference in predicted inner core age for the POLY and  
449 N14 models is  $\sim 50$  Myr, which is about 10% of the ages that are obtained below. More  
450 importantly, model N14C5 predicts that a dynamo persists for the last 3.5 Ga while the other  
451 models predict that the dynamo fails around the time of inner core nucleation. Both POLY  
452 and N14 models predict an older inner core than P12C6 indicating that the assumption of  
453 a constant cooling rate, which was used by P12 to calculate the inner core age, is not borne  
454 out by the evolution models.

455 There are two reasons for the similar behaviour of models POLYC4 and POLYC6 in  
456 Figure 3. First, the  $\Delta T_X$  computed using equation (18) are only weakly depth-dependent,  
457 partly because liquid and solid concentrations do not change significantly over time and  
458 partly because the increase of  $T_{\text{m,Fe}}$  with pressure is mostly offset by a decrease in  $\Delta S_{\text{Fe}}$   
459 with pressure. Second, S and Si contributions to the gravitational energy (and entropy) are

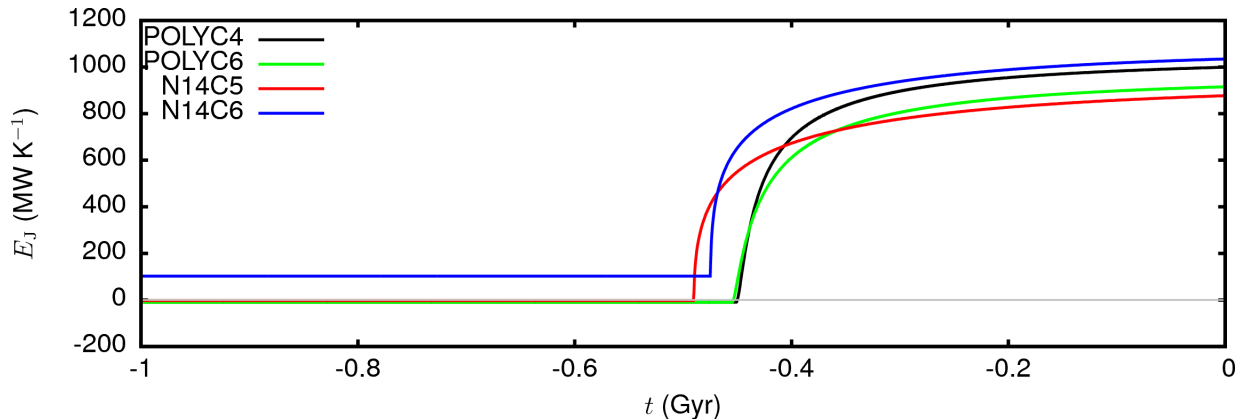


Figure 3: Power available to drive the dynamo  $E_J$  over time for the different models of core structure shown in Table 3. The present-day is at time  $t = 0$ .

460 at least an order of magnitude smaller than the contribution from O. An example of this  
 461 behaviour is shown in section 4.2 below.

462 We note that considering just the present-day energetics of the core suggests that Case  
 463 5 would generate a magnetic field for the whole of Earth’s history (Pozzo et al., 2012).  
 464 However, Figure 3 shows that there is insufficient power available to the dynamo before  
 465 inner core nucleation owing to the increase in conduction entropy with age. This example  
 466 shows the importance of analysing the whole cooling history rather than just the present-day  
 467 energy budget.

468 The heat of reaction and pressure heating were ignored in the calculations shown in  
 469 Figure 3 and Table 3 in order to compare with previous results. These terms were found  
 470 to be small in the present-day core energy budget (Gubbins et al., 2003, 2004). Table 4  
 471 shows how the inclusion of these terms affects the predicted inner core age and ancient core  
 472 temperature for the calculations in Table 3. The heat of reaction  $E_h$  makes no difference  
 473 to the results and can be safely ignored. Adding the pressure heating makes the inner core  
 474 25 Myr older than the calculations in Table 3 and decreases the ancient core temperature  
 475 by 10 K. We regard this difference as small and ignore the pressure heating terms from now  
 476 on. Table 4 also shows that changing the value of  $C_p$  from  $715 \text{ J kg}^{-1} \text{ K}^{-1}$  (used in this  
 477 study) to  $840 \text{ J kg}^{-1} \text{ K}^{-1}$  (used by (Nimmo, 2014)) increases the predicted inner core age  
 478 by 25 Myr and lowers the ancient core temperature by 175 K.

#### 479 4. Minimum entropy core cooling models

480 We now present models of marginal dynamo evolution, i.e. models with the minimum  
 481  $E_J$  such that  $E_J \geq 0$  for all time. Unless stated, results use model MG for core chemistry.  
 482 Results for models with different values of  $\Delta\rho$ ,  $h$  and  $k(r_o)$  are summarised in Figure 7.  
 483 Parameter values are listed in column 4 of Table 1.

| $C_p$ | $E_h$ ( $\text{W K}^{-1}$ ) | $Q_P + Q_{PL}$ (TW) | IC age (Myr) | $T_{an}$ (K) |
|-------|-----------------------------|---------------------|--------------|--------------|
| 715   | 0                           | 0                   | 451          | 5104         |
| 715   | 13                          | 0                   | 451          | 5104         |
| 715   | 0                           | 1.06                | 477          | 4994         |
| 840   | 0                           | 0                   | 477          | 4949         |
| 840   | 0                           | 1.00                | 510          | 4938         |

Table 4: Effect of changing the specific heat capacity  $C_p$ , heat of reaction  $E_h$  and pressure heating  $Q_P + Q_{PL}$  on predicted inner core age and core temperature at 3.5 Ga ( $T_{an}$ ) for the Case shown in Figure 3 and Table 3. The POLY core structure developed in section 2.1 has been used.

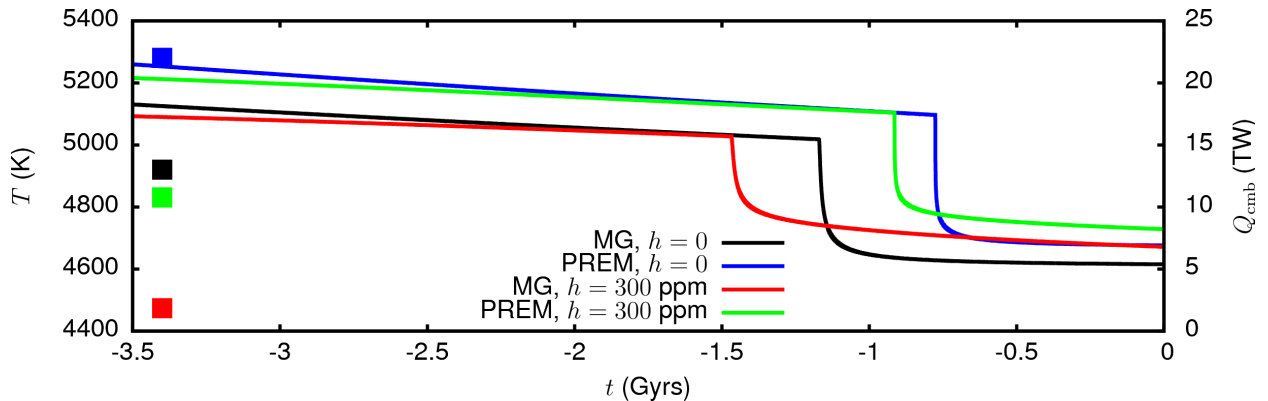


Figure 4: Marginal dynamo evolution with  $E_J = 0$  fixed in time.  $Q_{cmb} < Q_k$  during inner core solidification in these models. CMB heat-flux  $Q_{cmb}$  (solid lines) is plotted on the right ordinate; temperature at the top of the core at 3.5 Ga (squares) is plotted on the left ordinate. The present-day is at  $t = 0$ . Parameters are given in column 4 of Table 1. See text for details.

#### 4.1. Fixed Dynamo Power

Figure 4 shows the evolution of  $Q_{cmb}$  when  $E_J$  is set to zero for all time. The unrealistic jump in  $Q_{cmb}$  following inner core formation is clear. In these models  $Q_{cmb} < Q_k$  following inner core formation and so a stable region may be present at the top of the core. The larger density jump in model MG increases the gravitational energy, allowing the entropy budget to be balanced with a lower cooling rate than for model PREM. Cooling histories with the MG core model therefore predict an older inner core and lower ancient core temperature than those with the PREM core model. Adding radiogenic heating also slows down the cooling rate. The present-day CMB heat-flux required to sustain a marginal dynamo is in the range 5.5 – 8.5 TW; at 3.5 Ga,  $Q_{cmb} = 15 - 20$  TW. Predicted inner core ages range between 0.75 and 1.5 Ga. All models yield an ancient core temperature greater than 4400 K, which far exceeds estimates of  $4150 \pm 150$  K for the lower mantle solidus (Andraut et al., 2011)

Increasing  $E_J$  to ensure the core remains superadiabatic for the last 3.5 Ga strongly increases the power requirements. For the MG density jump and no radiogenic heating,  $E_J = 918 \text{ MW K}^{-1}$  is required to ensure  $Q_{cmb} > Q_k$ . The model predicts an inner core age of only 440 Myr and a very high CMB temperature of 7448 at 3.5 Ga.

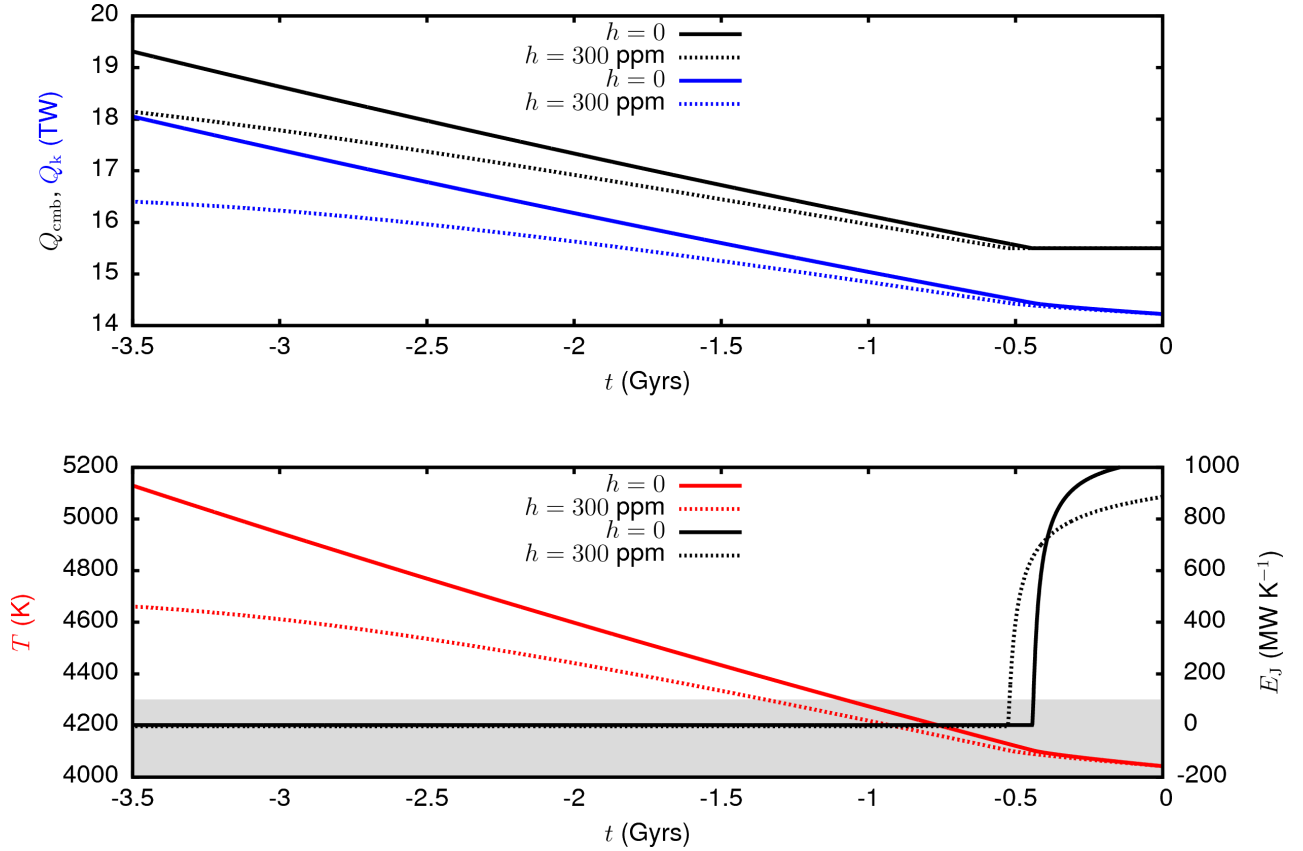


Figure 5: Marginal dynamo evolution with  $Q_{\text{cmb}}$  fixed during inner core growth and  $E_J$  fixed prior to inner core formation. Two models are shown:  $h = 0$  assumes no radiogenic heating;  $h = 300$  ppm assumes 300 ppm of  $^{40}\text{K}$  in the core at the present-day. Top panel: CMB heat-flux  $Q_{\text{cmb}}$  and heat conducted down the adiabatic gradient  $Q_k$ . Bottom panel: temperature at the top of the core is shown on the left ordinate;  $E_J$  is shown on the right ordinate. The grey shaded region shows the range of lower mantle solidus temperatures estimated by Andraut et al. (2011). The present-day is at  $t = 0$ . Parameters are given in Table 1. See text for details.

#### 501 4.2. Fixed CMB heat-flux

502 Figure 5 shows marginal dynamo evolution when  $Q_{\text{cmb}}$  is fixed during inner core growth  
503 and  $E_J$  is fixed prior to inner core formation.  $E_J$  increases rapidly during inner core growth  
504 because of latent heat and gravitational energy sources.  $Q_{\text{cmb}}$  always exceeds the adiabatic  
505 heat-flux  $Q_k$ , as it must for  $E_J$  to remain positive in this case. At the present-day, this cooling  
506 history yields a high CMB heat-flux of 15.5 TW. The inner core age is 444 Myr, while the  
507 ancient core temperature of 5130 K is very high. In this model the core temperature exceeds  
508 current estimates of the lower mantle solidus until around 1 Ga, suggesting that the lower  
509 mantle would be at least partially molten for most of Earth’s history.

510 Figure 5 also shows the model with minimum  $E_J$  that contains an additional 300 ppm  
511 of potassium at the present-day. As is well known (e.g. Nimmo et al., 2004), the addition  
512 of radiogenic heating slows core cooling while making only a small change to the entropy  
513 budget. Nevertheless, the model still predicts a young inner core age of 526 Myr and a high

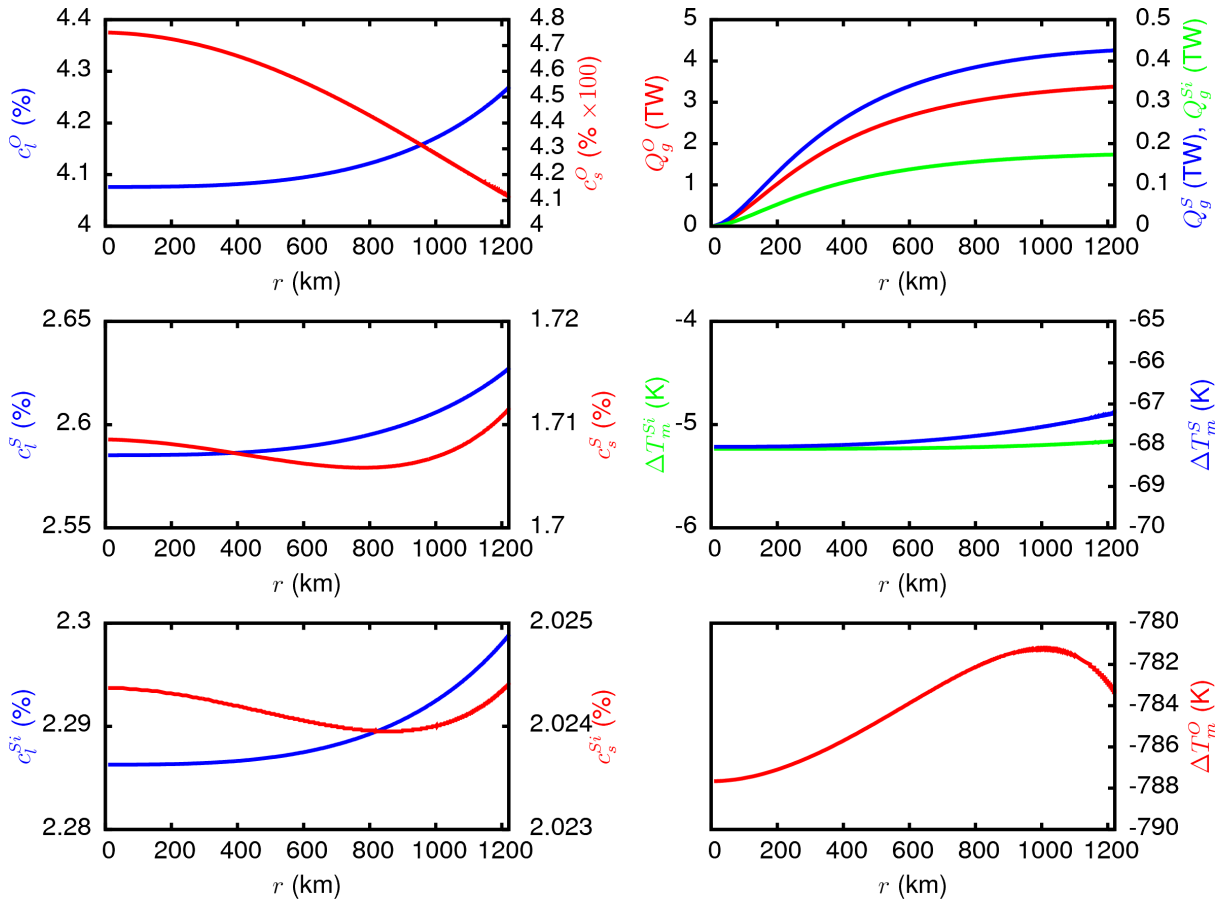


Figure 6: Effect of time-varying light element concentrations in the MG model of core chemistry. All quantities are plotted as functions of the inner core boundary radius,  $r$ . Top left: O concentration in the liquid (blue) and solid (red); middle left: S concentration in the liquid (blue) and solid (red); bottom left: Si concentration in the liquid (blue) and solid (red). All concentrations are given as mass fractions. Top right: contributions to the gravitational energy  $Q_g$  from O (red), S (blue) and Si (green); middle right: depression of the melting point due to Si (green) and S (blue); bottom right: depression of the melting point due to O (red). Note the different limits on the axes.

514 early core temperature of 4660 K. In this model the core temperature drops below the upper  
 515 estimate of 4300 K for the lower mantle solidus at 1350 Ma.

516 Figure 6 shows the partitioning and melting behaviour. The results are plotted against  
 517 inner core radius rather than time and hence apply to all models with the MG density jump.  
 518 Each of the light element concentrations vary by less than 5% of their present-day values over  
 519 the timescale of inner core growth. Almost all the O partitions into the liquid on freezing,  
 520 Si partitions almost equally and about 65% of the S goes into the liquid. The gravitational  
 521 energy is therefore dominated by the contribution from O, while the Si contribution is much  
 522 less than that of S. The melting point depression varies little with inner core radius because  
 523 the concentration changes are small. Again, O dominates the melting point depression,  
 524 while the contribution from Si is negligible. The presence of S depresses the melting point

525 by almost 70 K; given that the core cools by, say, 100 K over 1 Ga this contribution is  
526 significant.

527 Figure 7 plots inner core age against present-day CMB heat flow,  $Q_{\text{Pres}}$ , for a variety of  
528 marginal core histories with  $Q_{\text{cmb}}$  fixed during inner core growth and  $E_{\text{J}}$  fixed prior to inner  
529 core formation. Adding radiogenic heating, all other things being equal, increases the inner  
530 core age and slightly changes  $Q_{\text{Pres}}$ . Increasing the thermal conductivity at the top of the  
531 core substantially decreases the inner core age and increases  $Q_{\text{Pres}}$ : for model MG,  $h = 0$   
532 and  $k_0 = 90 \text{ W m}^{-1} \text{ K}^{-1}$  the inner core age is 480 Myr and  $Q_{\text{Pres}} = 14.4 \text{ TW}$  while the same  
533 model with  $k_0 = 110 \text{ W m}^{-1} \text{ K}^{-1}$  gives an age of 405 Myr and  $Q_{\text{Pres}} = 17.0 \text{ TW}$ . The PREM  
534 density jump gives a younger inner core and higher  $Q_{\text{Pres}}$  than the MG density jump.

535 Figure 7 also shows the core temperature at 3.5 Ga,  $T_{\text{an}}$ , plotted against the age  $t_s$   
536 (before present) when the core temperature fell below 4300 K, which is the highest value  
537 of the lower mantle solidus temperature using the error estimates of Andrault et al. (2011).  
538 Adding radiogenic heating increases  $t_s$  and decreases  $T_{\text{an}}$  while higher values of  $k_0$  decrease  $t_s$   
539 and increase  $T_{\text{an}}$ . The PREM density jump yields much lower values of  $t_s$  and slightly higher  
540 values of  $T_{\text{an}}$  than the MG density jump. The message from this Figure is that all cooling  
541 histories yield an inner core age younger than 600 Myr, and core temperature at 3.5 Ga that  
542 far exceeds present estimates of the lower mantle solidus temperature. All models suggest  
543 the lower mantle was at least partially molten until at least the last 1.5 Ga. Sustaining a  
544 marginal dynamo over the last 3.5 Ga with a superadiabatic core requires the present-day  
545 CMB heat flow to exceed  $\sim 14 \text{ TW}$ .

## 546 5. Discussion and conclusions

547 The cooling history of Earth's core has been investigated using a 4-component (iron plus  
548 oxygen, sulphur and silicon) analytical thermodynamic model. The study was motivated by  
549 recent upward revision of the thermal conductivity of liquid iron mixtures (de Koker et al.,  
550 2012; Pozzo et al., 2013; Gomi et al., 2013), which was previously found to drastically reduce  
551 the power available to the geodynamo at the present-day (Pozzo et al., 2012). Because the  
552 geomagnetic field is known to have survived for at least the last 3.45 Ga (Tarduno et al.,  
553 2010), core cooling histories that constrain the thermodynamic conditions under which the  
554 geodynamo can persist are crucial for obtaining a coherent picture of long-term geomagnetic  
555 field evolution.

556 There are three novel aspects to the present thermodynamic model. First, it uses a poly-  
557 nomial representation of radial core structure (density, temperature, etc) that gives a good  
558 fit to present-day profiles derived from seismological and mineralogical data. The analytical  
559 expressions derived from these profiles are shown to produce results for the core energy and  
560 entropy budgets in close agreement with previous studies that numerically integrated the  
561 raw data. Second, the model incorporates a pressure-dependent melting point depression  
562 that also depends on the time evolution of O, S, and Si concentrations in the solid and liquid.  
563 Labrosse (2014) has investigated partitioning of O and S and similar results are obtained  
564 here. The variation of Si in the solid follows that of S, falling at first before increasing,  
565 further supporting the view (Labrosse, 2014) that the inner core is compositionally stably



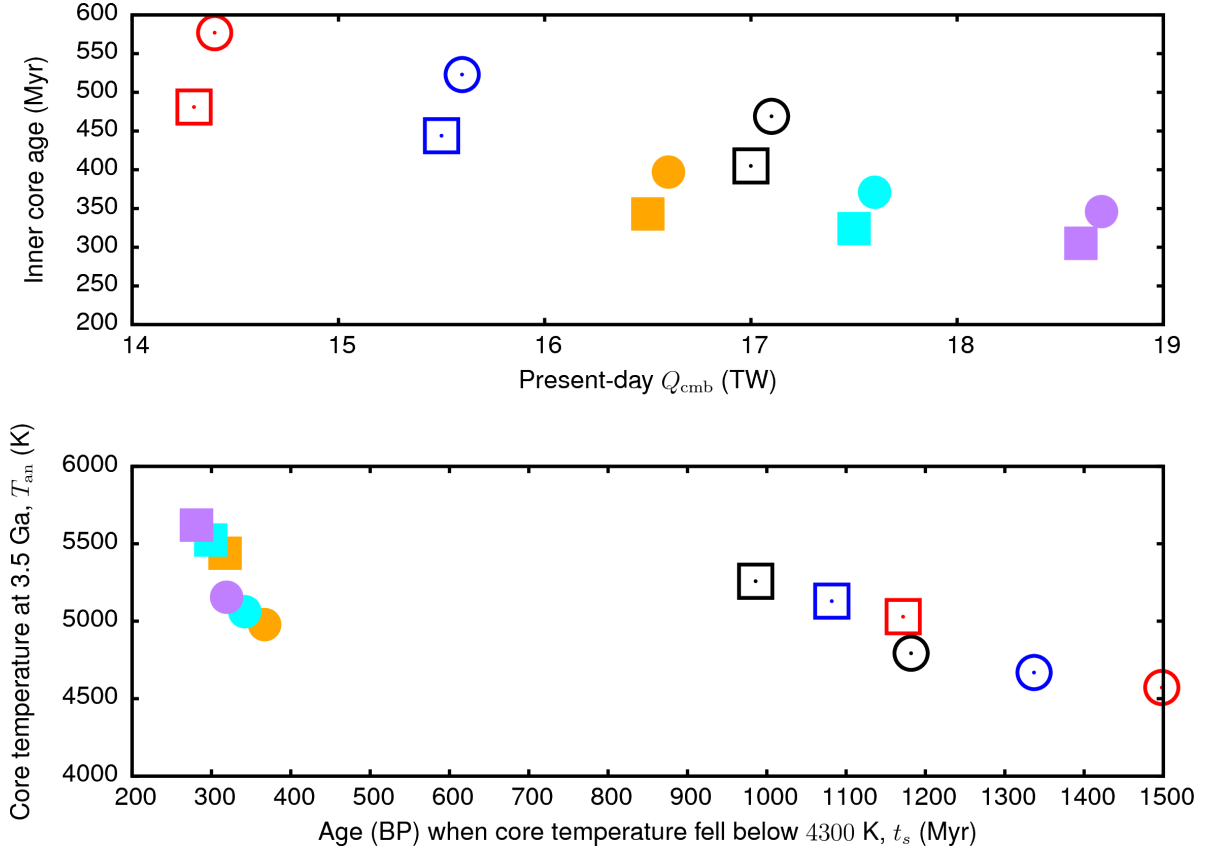


Figure 7: Phase diagram of present-day  $Q_{\text{cmb}}$  plotted against inner core age (top) and ancient core temperature  $T_{\text{an}}$  plotted against the age  $t_s$  where the core temperature fell below 4300 K (bottom). All cooling histories correspond to marginal dynamo evolution and have  $Q_{\text{cmb}}$  fixed during inner core growth and  $E_J$  fixed prior to inner core formation. Solid symbols denote cooling histories with the PREM core model; open symbols use the MG core model. Squares denote histories with  $h = 0$ ; circles denote histories with 300 ppm of  $^{40}\text{K}$  at the present-day. Colours show different values of the thermal conductivity at the top of the core: for model MG,  $k_0 = 90$  (red), 99 (blue) and 110 (black); for model PREM,  $k_0 = 100$  (orange), 107 (cyan) and 115 (purple).

566 stratified rather than unstable (Gubbins et al., 2013). Third, the gravitational energy re-  
567 leased by each light element is calculated. The contribution from O is dominant because  
568 almost all the O partitions into the liquid on freezing in the model of core chemistry adopted  
569 in this study.

570 The main results of the paper are summarised in Figure 7. All cooling histories have  
571 a young inner core, less than 600 Myr old, and core temperatures at 3.5 Ga between 4500  
572 and 5500 K. These results are broadly consistent with those obtained by Nimmo (2014)  
573 who found an inner core age of  $\leq 700$  Myrs and early core temperatures above 5000 K.  
574 Accounting for uncertainties in the input parameters such as the specific heat and the  
575 omission of pressure heating and heat of reaction (section 3) can increase the inner core age  
576 by  $\sim 50$  Myr and decrease the ancient core temperature by  $\sim 70$  K. However, even accounting  
577 for these uncertainties gives an inner core age much younger than the 1 Gyr obtained with  
578 old (low) values of the thermal conductivity (Labrosse et al., 2001) and a core primordial core  
579 temperature that far exceeds present estimates of  $4150 \pm 150$  K for the lower mantle solidus  
580 (e.g. Andrault et al., 2011). The core temperature in these cooling histories exceeded the  
581 lower mantle solidus for most of the last 3.5 Ga, dropping below it in the last 0.3–1.5 Myr.

582 It may be possible to obtain slower core cooling rates than those predicted in this study,  
583 but the options are not particularly appealing. One option is to increase the amount of  
584 radiogenic potassium in the core; however, the 300 ppm used in this study is on the upper  
585 end of present estimates (Nimmo, 2014) and some studies argue that there is no radioactive  
586 heating in the core at all (Davies, 2007). Another possibility is that the uppermost core is  
587 strongly subadiabatic (see Figure 4). Pozzo et al. (2012) and Gomi et al. (2013) suggest that  
588 this scenario will involve a stable layer at the top of the core that is hundreds of kilometres  
589 thick, which is likely to be inconsistent with geomagnetic secular variation (Gubbins, 2007;  
590 Buffett, 2014). Moreover, the cooling histories in Figure 4 have early core temperatures  
591 in excess of 4300 K even though they have the Ohmic heating  $E_J = 0$  for all time. A  
592 third option is that the density jump at the inner core boundary (ICB) is higher than the  
593  $\Delta\rho = 0.6, 0.8 \text{ g cc}^{-1}$  used in this work. Masters and Gubbins (2003) find  $\Delta\rho = 0.8 \pm 0.2$   
594  $\text{g cc}^{-1}$ . However, if the trend between cooling histories with  $\Delta\rho = 0.6$  and  $0.8 \text{ g cc}^{-1}$  in  
595 Figure 7 persists up to  $\Delta\rho = 1 \text{ g cc}^{-1}$  the predicted inner core age will still be significantly  
596 less than 1 Gyr and the ancient core temperature will exceed 4300 K. A fourth option is to  
597 use different models of core chemistry. We have assumed equal amounts of S and Si for each  
598 density jump, but other options are possible. Moreover, other elements such as H (Nomura  
599 et al., 2014) could be present in the core. The formalism presented above for computing  
600 partition coefficients and the melting point depression can be applied to any core chemistry  
601 model where the light elements behave independently. At present, testing this option require  
602 more data from mineral physics. Finally, it should be noted that there is still uncertainty in  
603 the adiabatic temperature and the melting curve for pure iron, which affect the calculated  
604 inner core growth rate and melting point depression. One set of temperature profiles have  
605 been adopted for this study. Future work will consider the effect of other choices.

606 The models in this study correspond to a state of marginal dynamo evolution, i.e. they  
607 yield the minimum  $E_J$  such that  $E_J \geq 0$  for all time. In the Earth’s core  $E_J$  certainly  
608 exceeds that for a marginal dynamo at the present-day and probably has done for the last

609 3.5 Ga (e.g. Roberts et al., 2003; Gubbins et al., 2003). Higher values of  $E_J$  require higher  
610 core cooling rates to balance the entropy budget, resulting in higher core-mantle boundary  
611 (CMB) heat flows, a younger inner core age and a hotter primordial core than the estimates  
612 given here. Putting  $E_J \sim 10^8 \text{ W K}^{-1}$  (Roberts et al., 2003) will easily offset any decrease  
613 in cooling rate that could be found from the options suggested about. It therefore seems  
614 inevitable that future models of coupled core-mantle evolution must contend with high CMB  
615 heat flows, high core temperatures, long-lived partial melting at the base of the mantle, and  
616 possibly stratification at the top of the core.

617 A high present-day CMB heat flow of  $> 14 \text{ TW}$  is needed to maintain the geodynamo  
618 unless the top of the core is subadiabatic in which case 6–9 TW ensures a marginal dynamo.  
619 At 3.5 Ga CMB heat flows of  $\sim 15 \text{ TW}$  are needed to maintain a marginal dynamo. We  
620 also note that cooling histories with the PREM ICB density jump require present-day CMB  
621 in the range 16–18 TW depending on the thermal conductivity. Pozzo et al. (2013) find  
622  $k = 99 \text{ W m}^{-1} \text{ K}^{-1}$  at the CMB for the PREM ICB density jump; if this value is an under-  
623 estimate, the CMB heat flow required to maintain an adiabatic core will exceed independent  
624 estimates of 7–17 TW for CMB heat flow (Lay et al., 2009; Nimmo, 2014).

625 The high primordial core temperatures are consistent with models of an ancient magma  
626 ocean at the base of the mantle. Labrosse et al. (2007) and Ziegler and Stegman (2013)  
627 both propose models that have a molten lowermost mantle at the present-day, although the  
628 thickness of their molten layers are rather different. However, the possibility that such a  
629 magma ocean would thermally insulate the core (Labrosse et al., 2007) raises the question  
630 of whether the core can cool rapidly enough beneath this thermal blanket to sustain the  
631 magnetic field at early times. Chemical exchange may also take place between the core and  
632 magma ocean. If this occurs then the direction of exchange will likely be crucial for early core  
633 dynamics; emplacing light material at the top of the core would lead to chemical stratification  
634 unless existing convection could mix the heterogeneity. Modelling the simultaneous evolution  
635 of core and magma ocean should shed light on the viability of an early core dynamo.

## 636 Acknowledgements

637 C.D. is supported by Natural Environment Research Council fellowships NE/H01571X/1  
638 and NE/L011328/1 and a fellowship from the Green Foundation at IGPP, Scripps Institution  
639 of Oceanography. The author thanks Prof. Dario Alfè for providing data and Prof. Francis  
640 Nimmo for many valuable discussions. The use of a polynomial representation of core struc-  
641 ture was motivated by stimulating discussions with John Hernlund, Stéphane Labrosse and  
642 David Gubbins at the Onsen II meeting in Tokyo, Japan (October 2013). The construc-  
643 tive and detailed comments of Stéphane Labrosse and an anonymous reviewer are gratefully  
644 acknowledged.

## 645 Appendix

646 This Appendix contains analytical expressions for the integrals in equations (5) derived  
647 from the polynomial expressions for radial core structure given in section 2. The integrals

648 in the entropy terms  $E_a$ ,  $E_k$  and  $E_r$  are of the form  $X(r)/T_a(r)$  and hence the analytical  
649 expressions are very long. We present the results for  $E_r$  below; the derivations of  $E_a$  and  $E_k$   
650 are similar. In practice it is just as easy to numerically integral  $E_a$ ,  $E_k$  and  $E_r$ . Both  
651 approaches have been attempted here and the results are very similar.

### 652 *Secular Cooling*

The secular cooling term is given by

$$Q_s = -\frac{C_p}{T_o} \int \rho(r)T_a(r)dV \frac{dT_o}{dt} = -4\pi \frac{C_p}{T_o} \int_0^{r_o} \rho(r)T_a(r)r^2 dr \frac{dT_o}{dt}.$$

Using equations (7) and (15) the integral can be written as

$$\int \rho(r)T_a(r)dV = 4\pi [S_o(r_o) - S_o(r_i) + S_i(r_i)],$$

where

$$S_o(r) = \frac{s_1^o}{3}r^3 + \frac{s_2^o}{4}r^4 + \frac{s_3^o}{5}r^5 + \frac{s_4^o}{6}r^6 + \frac{s_5^o}{7}r^7 + \frac{s_6^o}{8}r^8 + \frac{s_7^o}{9}r^9,$$

and

$$S_i(r) = \frac{s_1^i}{3}r^3 + \frac{s_2^i}{4}r^4 + \frac{s_3^i}{5}r^5 + \frac{s_4^i}{6}r^6 + \frac{s_5^i}{7}r^7 + \frac{s_6^i}{8}r^8.$$

Here

$$\begin{aligned} s_1^o &= \rho_0^{\text{oc}}T_{\text{cen}}, \\ s_2^o &= \rho_0^{\text{oc}}T_{\text{cen}}t_1 + \rho_1^{\text{oc}}T_{\text{cen}}, \\ s_3^o &= \rho_2^{\text{oc}}T_{\text{cen}} + \rho_1^{\text{oc}}T_{\text{cen}}t_1 + \rho_0^{\text{oc}}T_{\text{cent}2}, \\ s_4^o &= \rho_3^{\text{oc}}T_{\text{cen}} + \rho_2^{\text{oc}}T_{\text{cent}1} + \rho_1^{\text{oc}}T_{\text{cent}2} + \rho_0^{\text{oc}}T_{\text{cent}3}, \\ s_5^o &= \rho_3^{\text{oc}}T_{\text{cent}1} + \rho_2^{\text{oc}}T_{\text{cent}2} + \rho_1^{\text{oc}}T_{\text{cent}3}, \\ s_6^o &= \rho_3^{\text{oc}}T_{\text{cent}2} + \rho_2^{\text{oc}}T_{\text{cent}3}, \\ s_7^o &= \rho_3^{\text{oc}}T_{\text{cent}3}, \end{aligned}$$

and

$$\begin{aligned} s_1^i &= \rho_0^{\text{ic}}T_{\text{cen}}, \\ s_2^i &= \rho_0^{\text{ic}}T_{\text{cent}1}, \\ s_3^i &= \rho_2^{\text{ic}}T_{\text{cen}} + \rho_0^{\text{ic}}T_{\text{cent}2}, \\ s_4^i &= \rho_2^{\text{ic}}T_{\text{cent}1} + \rho_0^{\text{ic}}T_{\text{cent}3}, \\ s_5^i &= \rho_2^{\text{ic}}T_{\text{cent}2}, \\ s_6^i &= \rho_2^{\text{oc}}T_{\text{cent}3}. \end{aligned}$$

653 *Gravitational energy*

Gubbins et al. (2004) shows that

$$Q_g = \alpha_c \frac{Dc_X^l}{Dt} \int \rho(r)\psi(r)dV = \alpha_c \frac{Dc_X^l}{Dt} \left[ 4\pi \int_{r_i}^{r_o} \rho(r)\psi(r)r^2 dr - M_{oc}\psi(r_i) \right].$$

654 Using equations (7) and (12) we find

$$\int \rho(r)\psi(r)dV_{oc} = 16\pi^2 G [G_c(r_o) - G_c(r_i) + G_b(r_o) - G_b(r_i)] \quad (28)$$

655 where

$$G_c(r) = g_1^o r^5 + g_2^o r^6 + g_3^o r^7 + g_4^o r^8 + g_5^o r^9 + g_6^o r^{10} + g_7^o r^{11} \quad (29)$$

656 and

$$G_b(r) = \psi(r_o) \left( \frac{\rho_0^{oc}}{3} r^3 + \frac{\rho_1^{oc}}{4} r^4 + \frac{\rho_2^{oc}}{5} r^5 + \frac{\rho_3^{oc}}{6} r^6 \right) \quad (30)$$

where

$$\begin{aligned} g_1^o &= \rho_0^{oc^2}/30, \\ g_2^o &= \rho_0^{oc} \rho_1^{oc}/24, \\ g_3^o &= \rho_1^{oc^2}/84 + \rho_0^{oc} \rho_2^{oc} 13/420, \\ g_4^o &= \rho_1^{oc} \rho_2^{oc} / + \rho_0^{oc} \rho_3^{oc} /40, \\ g_5^o &= \rho_2^{oc^2}/180 + 7\rho_1^{oc} \rho_3^{oc} /540, \\ g_6^o &= \rho_2^{oc} \rho_3^{oc} /120, \\ g_7^o &= \rho_3^{oc^2} /330. \end{aligned}$$

657 *Pressure Heating*

The density differential can be written in terms of concentration, temperature and pressure:

$$d\rho = \left( \frac{\partial \rho}{\partial c} \right)_{P,T} dc + \left( \frac{\partial \rho}{\partial T} \right)_{P,c} dT + \left( \frac{\partial \rho}{\partial P} \right)_{c,T} dP.$$

We follow Gubbins et al. (1979) and use a simplified implementation of the pressure heating  $Q_P$  that neglects the thermal and pressure effects on density so that

$$\frac{D\rho}{Dt} = \rho \alpha_c \frac{Dc}{Dt}.$$

658 These approximations are justified by the smallness of  $Q_P$  and its associated entropy  $E_P$ .  
 659 Moreover, the results obtained here give good agreement with those obtained by Gubbins  
 660 et al. (2003), who performed a more complex calculation.

Differentiating the hydrostatic equation (13) gives

$$\begin{aligned}\frac{DP}{Dt} &= - \int_{r_o}^r \frac{D\rho}{Dt} \frac{4\pi G}{r^2} \left[ \int_0^r \rho r'^2 dr' \right] dr - \int_{r_o}^r \frac{4\pi G \rho}{r^2} \left[ \int_0^r \frac{D\rho}{Dt} r'^2 dr' \right] dr + \frac{DP}{Dt}(r_o), \\ &= 8\pi G \alpha_c \frac{Dc}{Dt} \int_{r_o}^r \frac{\rho}{r^2} \left[ \int_0^r \rho r'^2 dr' \right] dr + \frac{DP}{Dt}(r_o).\end{aligned}$$

661 The integral can be evaluated using equation (7) using the procedure to calculate the mass  
662 of the core [equation 9].

### 663 *Radiogenic Heating*

The entropy due to radiogenic heating depends on the integral

$$\int \frac{\rho(r)}{T_a(r)} dV = 4\pi \int_0^{r_o} \frac{\rho(r)}{T_a(r)} r^2 dr.$$

This integral can be evaluated by long division and then partial fractions on the remainder. The result is

$$\int \frac{\rho}{T_a} dV = 4\pi \left[ \frac{A_3}{3} r_o + \frac{B_3}{2t_3} r_o^2 + \frac{C_3}{t_3} r_o + X \log(r_o - R_1) + Y \log(r_o - R_2) + Z \log(r_o - R_3) \right].$$

where

$$A = \frac{\rho_3^{oc}}{t_3}; B_i = (\rho_i - At_i); C_i = B_i - \frac{B_3}{t_3} t_i; D_i = C_i - \frac{C_3}{t_3} t_i.$$

Here the index  $i$  runs from 0 to 2. The quantities  $X$ ,  $Y$  and  $Z$  are given by

$$\begin{aligned}Z &= \left[ D_2 - D_3(R_3 + R_2) - (R_1 - R_2) - (R_1 - R_2) \left( \frac{D_1 + D_3 R_2 R_3}{(R_2 R_3 - R_1 R_3)} \right) \right] \times \\ &\quad \left[ (R_1 - R_3) + (R_2 - R_1) \left( \frac{R_2 R_3 - R_1 R_2}{R_2 R_3 - R_1 R_3} \right) \right]^{-1}, \\ Y &= \frac{D_1 + D_3 R_2 R_3 - C(R_2 R_3 - R_1 R_2)}{(R_2 R_3 - R_1 R_3)}, \\ X &= D_3 - B - C.\end{aligned}$$

664 Here  $R_1$ ,  $R_2$  and  $R_3$  are the three roots of  $T_a(r)$ .

665 **References**

- 666 Alfé, D., Gillan, M., Price, G., 2002a. Ab initio chemical potentials of solid and liquid solutions and the  
667 chemistry of the Earth’s core. *J. Chem. Res.* 116, 7127–7136.
- 668 Alfé, D., Gillan, M., Price, G., 2002b. Composition and temperature of the Earth’s core constrained by  
669 combining ab initio calculations and seismic data. *Earth Planet. Sci. Lett.* 195, 91–98.
- 670 Alfé, D., Gillan, M. J., Price, G. D., 2007. Temperature and composition of the Earth’s core. *Contemp.*  
671 *Phys.* 48, 63–80.
- 672 Alfé, D., Price, G., Gillan, M., 2002c. Iron under Earth’s core conditions: Liquid-state thermodynamics and  
673 high-pressure melting curve from ab initio calculations. *Phys. Rev. B* 65, 165118.
- 674 Andraut, D., Bolfan-Casanova, N., Lo Nigro, G., Bouhifd, M., Garbarinho, G., Mezouar, M., 2011. Solidus  
675 and liquidus profiles of chondritic mantle: Implication for melting of the Earth across its history. *Earth*  
676 *Planet. Sci. Lett.* 304, 251–259.
- 677 Biggin, A., Strik, G., Langereis, C., 2009. The intensity of the geomagnetic field in the late-Archaeon: new  
678 measurements and an analysis of the updated IAGA palaeointensity database. *Earth Planets Space* 61,  
679 9–22.
- 680 Braginsky, S., 1963. Structure of the F layer and reasons for convection in the Earth’s core. *Sov. Phys. Dokl.*  
681 149, 8–10.
- 682 Braginsky, S., Roberts, P., 1995. Equations governing convection in Earth’s core and the geodynamo. *Geo-*  
683 *phys. Astrophys. Fluid Dyn.* 79, 1–97.
- 684 Buffett, B., 2002. Estimates of heat flow in the deep mantle based on the power requirements for the  
685 geodynamo. *Geophys. Res. Lett.* 29, 10.1029/2001GL014649.
- 686 Buffett, B., 2009. Onset and orientation of convection in the inner core. *Geophys. J. Int.* 179, 711–719.
- 687 Buffett, B., 2012. Earth science: Geomagnetism under scrutiny. *Nature* 485, 319–320.
- 688 Buffett, B., 2014. Geomagnetic fluctuations reveal stable stratification at the top of the Earth’s core. *Nature*  
689 507, 484–487.
- 690 Buffett, B., Huppert, H., Lister, J., Woods, A., 1996. On the thermal evolution of the Earth’s core. *J.*  
691 *Geophys. Res.* 101, 7989–8006.
- 692 Davies, C., Gubbins, D., 2011. A buoyancy profile for the Earth’s core. *Geophys. J. Int.* 187, 549–563.
- 693 Davies, G., 2007. Mantle regulation of core cooling: A geodynamo without core radioactivity? *Phys. Earth*  
694 *Planet. Int.* 160, 215–229.
- 695 de Koker, N., Steinle-Neumann, G., Vojtech, V., 2012. Electrical resistivity and thermal conductivity of  
696 liquid Fe alloys at high P and T and heat flux in Earth’s core. *Proc. Natl. Acad. Sci.* 109, 4070–4073.
- 697 Dziewonski, A., Anderson, D., 1981. Preliminary Reference Earth Model. *Phys. Earth Planet. Int.* 25, 297–  
698 356.
- 699 Fiquet, G., Auzende, A., Siebert, J., Corgne, A., Bureau, H., Ozawa, H., Garbarino, G., 2010. Melting of  
700 peridotite to 140 gigapascals. *Science* 329, 1516–1518.
- 701 Gomi, H., Ohta, K., Hirose, K., Labrosse, S., Caracas, R., Verstraete, V., Hernlund, J., 2013. The high  
702 conductivity of iron and thermal evolution of the Earth’s core. *Phys. Earth Planet. Int.* 224, 88–103.
- 703 Gubbins, D., 1975. Can the Earth’s magnetic field be sustained by core oscillations? *Geophys. Res. Lett.* 2,  
704 409–412.
- 705 Gubbins, D., 2007. Geomagnetic constraints on stratification at the top of Earth’s core. *Earth Planets Space*  
706 59, 661–664.
- 707 Gubbins, D., Alfé, D., Davies, C., 2013. Compositional instability of Earth’s solid inner core. *Geophys. Res.*  
708 *Lett.* 40, 1084–1088.
- 709 Gubbins, D., Alfé, D., Masters, G., Price, G., Gillan, M., 2003. Can the Earth’s dynamo run on heat alone?  
710 *Geophys. J. Int.* 155, 609–622.
- 711 Gubbins, D., Alfé, D., Masters, G., Price, G., Gillan, M., 2004. Gross thermodynamics of two-component  
712 core convection. *Geophys. J. Int.* 157, 1407–1414.
- 713 Gubbins, D., Masters, T., Jacobs, J., 1979. Thermal evolution of the Earth’s core. *Geophys. J. R. Astr. Soc.*  
714 59, 57–99.

- 715 Hirose, K., Labrosse, S., Hernlund, J., 2013. Compositional state of Earth's core. *Annual Review of Earth*  
716 *and Planetary Sciences* 41, 657–691.
- 717 Jaupart, C., Labrosse, S., Mareschal, J.-C., 2007. Temperatures, heat and energy in the mantle of the Earth.  
718 In: Schubert, G. (Ed.), *Treatise on Geophysics*, Vol. 7. Elsevier, Amsterdam, pp. 254–303.
- 719 Labrosse, S., 2003. Thermal and magnetic evolution of the Earth's core. *Phys. Earth Planet. Int.* 140,  
720 127–143.
- 721 Labrosse, S., 2014. Thermal and compositional stratification of the inner core. *C. R. Acad. Sci. Paris*.
- 722 Labrosse, S., Hernlund, J., Coltice, N., 2007. A crystallizing dense magma ocean at the base of the Earth's  
723 mantle. *Nature* 450, 866–869.
- 724 Labrosse, S., Poirier, J.-P., Le Moeul, J.-L., 1997. On cooling of the Earth's core. *Phys. Earth Planet. Int.*  
725 99, 1–17.
- 726 Labrosse, S., Poirier, J.-P., Le Moeul, J.-L., 2001. The age of the inner core. *Earth Planet. Sci. Lett.* 190,  
727 111–123.
- 728 Lay, T., Hernlund, J., Buffett, B., 2009. Core-mantle boundary heat flow. *Nat. Geosci.* 1, 25–32.
- 729 Lister, J., 2003. Expressions for the dissipation driven by convection in the Earth's core. *Phys. Earth Planet.*  
730 *Int.* 140, 145–158.
- 731 Lister, J., Buffett, B., 1995. The strength and efficiency of thermal and compositional convection in the  
732 geodynamo. *Phys. Earth Planet. Int.* 91, 17–30.
- 733 Lister, J., Buffett, B., 1998. Stratification of the outer core at the core-mantle boundary. *Phys. Earth Planet.*  
734 *Int.* 105, 5–19.
- 735 Loper, D., 1978. Some thermal consequences of a gravitationally powered dynamo. *J. Geophys. Res.* 831.
- 736 Manglik, A., Wicht, J., Christensen, U., 2010. A dynamo model with double diffusive convection for Mer-  
737 cury's core. *Earth Planet. Sci. Lett.* 209, 619–628.
- 738 Masters, G., Gubbins, D., 2003. On the resolution of density within the Earth. *Phys. Earth Planet. Int.* 140,  
739 159–167.
- 740 Nakagawa, T., Tackley, P., 2013. Implications of high core thermal conductivity on Earth's coupled mantle  
741 and core evolution. *Geophys. Res. Lett.* 40, 1–5.
- 742 Nakagawa, T., Tackley, P., 2014. Influence of combined primordial layering and recycled MORB on the  
743 coupled thermal evolution of Earth's mantle and core. *Geochem. Geophys. Geosys.* 15, 619–633.
- 744 Nimmo, F., 2007. Thermal and compositional evolution of the core. In: Schubert, G. (Ed.), *Treatise on*  
745 *Geophysics*, Vol. 9. Elsevier, Amsterdam, pp. 217–241.
- 746 Nimmo, F., 2014. Energetics of the core. In: Schubert, G. (Ed.), *Treatise on Geophysics 2nd Edn*, Vol. 9.  
747 Elsevier, Amsterdam, pp. 31–65.
- 748 Nimmo, F., Price, G., Brodholt, J., Gubbins, D., 2004. The influence of potassium on core and geodynamo  
749 evolution. *Geophys. J. Int.* 156, 363–376.
- 750 Nomura, R., Hirose, K., Uesugi, K., Ohishi, Y., Tsuchiyama, A., Miyake, A., Ueno, Y., 2014. Low core-  
751 mantle boundary temperature inferred from the solidus of pyrolite. *Science* 343, 522–524.
- 752 Poirier, J.-P., 1994. *Introduction to the physics of Earth's interior*, 2nd Edition. Cambridge University Press.
- 753 Pozzo, M., Davies, C., Gubbins, D., Alfè, D., 2012. Thermal and electrical conductivity of iron at Earth's  
754 core conditions. *Nature* 485, 355–358.
- 755 Pozzo, M., Davies, C., Gubbins, D., Alfè, D., 2013. Transport properties for liquid silicon-oxygen-iron  
756 mixtures at Earth's core conditions. *Phys. Rev. B* 87, 014110.
- 757 Pozzo, M., Davies, C., Gubbins, D., Alfè, D., 2014. Thermal and electrical conductivity of solid iron and  
758 iron-silicon mixtures at Earth's core conditions. *Earth Planet. Sci. Lett.* 393, 159–164.
- 759 Roberts, P., Jones, C., Calderwood, A., 2003. Energy fluxes and ohmic dissipation in the Earth's core. In:  
760 *Earth's core and lower mantle. Contributions from the SEDI 2000, The 7th Symposium*, pp. 100–129.
- 761 Stacey, F., 2007. Core properties, physical. In: Gubbins, D., Herrero-Bervera, E. (Eds.), *Encyclopedia of*  
762 *Geomagnetism and Paleomagnetism*. Springer, pp. 91–94.
- 763 Stacey, F., Anderson, O., 2001. Electrical and thermal conductivities of Fe-Ni-Si alloy under core conditions.  
764 *Phys. Earth Planet. Int.* 124, 153–162.
- 765 Stacey, F., Loper, D., 2007. A revised estimate of the conductivity of iron alloy at high pressure and



766 implications for the core energy balance. *Phys. Earth Planet. Int.* 161, 13–18.  
767 Stevenson, D., 1987. Limits on lateral density and velocity variations in the Earth's outer core. *Geophys. J.*  
768 *Int.* 88, 311–319.  
769 Tarduno, J., Cottrell, R., Watkeys, M., Hofmann, A., Doubrovine, P., Mamajek, E., Liu, D., Sibeck, D.,  
770 Neukirch, L., Usui, Y., 2010. Geodynamo, solar wind, and magnetopause 3.4 to 3.45 billion years ago.  
771 *Science* 327, 1238–1240.  
772 Verhoogen, J., 1961. Heat balance of the Earth's core. *Geophys. J. R. Astr. Soc.* 4, 276–281.  
773 Ziegler, L. B., Stegman, D. R., 2013. Implications of a long-lived basal magma ocean in generating Earth's  
774 ancient magnetic field. *Geochem. Geophys. Geosys.* 14, 4735–4742.